NEUROSCIENCE

Callosal inputs generate side-invariant receptive fields in the barrel cortex

Roberto Montanari, Javier Alegre-Cortés†, Alicia Alonso-Andrés†, Jorge Cabrera-Moreno, Ismael Navarro, Cristina García-Frigola, María Sáez, Ramón Reig*

Barrel cortex integrates contra- and ipsilateral whiskers' inputs. While contralateral inputs depend on the thalamocortical innervation, ipsilateral ones are thought to rely on callosal axons. These are more abundant in the barrel cortex region bordering with S2 and containing the row A-whiskers representation, the row lying nearest to the facial midline. Here, we ask what role this callosal axonal arrangement plays in ipsilateral tactile signaling. We found that novel object exploration with ipsilateral whiskers confines c-Fos expression within the highly callosal subregion. Targeting this area with in vivo patch-clamp recordings revealed neurons with uniquely strong ipsilateral responses dependent on the corpus callosum, as assessed by tetrodotoxin silencing and by optogenetic activation of the contralateral hemisphere. Still, in this area, stimulation of contra- or ipsilateral row A-whiskers evoked an indistinguishable response in some neurons, mostly located in layers 5/6, indicating their involvement in the midline representation of the whiskers' sensory space.

INTRODUCTION

The corpus callosum (CC) is the characteristic commissure of placental mammals' brains (*1*). The CC is mainly composed of glutamatergic axons interconnecting the two hemispheres and belonging to neocortical pyramidal neurons (*2*, *3*). Besides allowing the transfer of simple discriminative memories from the trained to the untrained hemisphere (*4*), the CC participates in motor and sensory operations. More specifically, in primary visual and somatosensory cortex (S1), it is involved in the fusion at the midline of the right and left sensory hemispaces (*5*–*9*). Accordingly, neurons dedicated to the midline of the visual and somatosensory space exhibit a side-invariant receptive field (RF). Namely, they manifest comparable sensitivity to the stimulation of sensory organs on either side of the body. This effect is obtained through the CC that replicates the primary thalamocortical response of the activated hemisphere into the opposite hemisphere, thus generating in the latter a mirror replica of the activation that occurred in the former (*6*). By generating side-invariant RFs, midline-crossing circuits would guarantee a continuity between the right and left sensory maps (*9*, *10*). Congruently, with this binding role, in S1 of placental mammals, side-invariant neurons represent midline and para-midline body regions like nose, chin, intraoral surfaces, ventral/dorsal trunk etc. and often occupy cytoarchitectonic borders of neocortical areas (*6*). On the contrary, in representations of body parts far from the midline (e.g., extremities), callosal connections are scant or absent [but see *7*)].

Rodent whiskers are somatotopically represented in the barrel cortex (BC). Thalamic innervation enables BC neurons to respond to contralateral whisker stimulations, while ipsilateral responses are commonly attributed to callosal innervation given the complete decussation of the trigeminothalamic tract (*11*–*16*). In rodents' BC, callosal innervation is scant and involves supra- and infragranular layers, for both axonal origin and termination (*17*). Axons entering from the white matter ascend toward the neocortical surface through septal dysgranular areas, extensively avoiding layer (L) 4 barrel hollows (*18*, *19*). The densest innervation is restricted to a narrow stripe at the S1/S2 cytoarchitectonic border (*18*–*25*). In the BC, this border contains the representation of row A-whiskers, the row that lies nearest to the facial midline (*22*, *23*). This resembles the S1 representation of other midline and para-midline body parts and led us to ask (i) how the interhemispheric synaptic transmission varies across distant regions of the BC that display different degrees of CC innervation and (ii) whether the whisker system also shows side-invariant RFs obeying the midline rule.

Our strategy involved testing the functional relevance of callosal axons' disposition in the BC by c-Fos activation in mice exploring novel objects with ipsilateral whiskers inputs only. Then, through in vivo whole-cell patch-clamp, we compared whisker responses in distal regions of the BC representing either para-midline (row A) or lateral (row E) whiskers. We found stronger and faster ipsilateral responses upon row A stimulation that were produced by the presynaptic excitation generated by the opposite hemisphere through the CC. Last, we report the presence of side-invariant responses dependent on the CC, which demonstrates that the whisker system conforms to the midline rule.

RESULTS

Ipsilateral whiskers induce regionalized c-Fos expression in the BC upon exploration

Whiskers-mediated tactile experience drives the somatotopic expression of c-Fos in the BC (*26*), indicating the metabolic activation of whiskers-dedicated neurons. The BC can respond to the stimulation of ipsilateral whiskers (*11*–*16*), but how the arrangement of callosal innervation affects its recruitment is unknown. First, we studied the arrangement of callosal projections in the BC by biotin dextran amide (BDA) injections in the opposite BC′. Injections restricted to the posterolateral aspect (i.e., row A/B territory) of the BC showed higher axonal density at homotopic locations in

Instituto de Neurociencias UMH-CSIC (Alicante), Avenida Santiago Ramón y Cajal s. n., 03550, Spain.
*Corresponding author. Email: ramon.reig@umh.es
†These authors contributed equally to this work.

the opposite BC′ than injections restricted to the anteromedial aspect (i.e., row D/E territory) (Fig. 1, A to C). This result confirmed the patterned disposition of callosal axons connecting the BCs. To explore the functional significance of this disposition, we extracted the density of c-Fos$^+$ expression in the BC of mice that were subjected to manipulations of their whisker arrays and to a subsequent period of free arena exploration with novel objects. Density of c-Fos$^+$ nuclei was quantified on flattened cortical preparations showing barrels′ outlines (see Materials and Methods). To avoid confusing the thalamocortical activity evoked by the contralateral whiskers with that evoked by the ipsilateral whiskers, we first looked for a method to isolate the BC from peripheral inputs of both sides. Hence, we trimmed the whiskers bilaterally at their base (Fig. 1E; n_{hem} = 10, two hemispheres per mouse). However, the density of c-Fos$^+$ nuclei across the BCs in this condition (table S1) did not differ from the control condition in which mice (Fig. 1D; n_{hem} = 6, two hemispheres per mouse) retained the entire set of bilateral whiskers (Fig. 1H; P = 0.3132). These two conditions only differed in the extent of c-Fos expression for anterior and posterior whiskers representation (fig. S1, A and B). Thus, BCs were still recruited despite the complete trimming of whiskers, indicating that this method could not be used to isolate the ipsilateral component of the BC activity. Subcutaneous injection of lidocaine in the whisker pad is a previously described method for long-lasting suppression of whisker responses in the BC (*27*). Lidocaine administration did not alter mice locomotor activity, measured as the total path and pauses during the task (fig. S1, C and D). In mice receiving lidocaine bilaterally (n_{hem} = 8, two hemispheres per mouse), BCs were nearly devoid of c-Fos expression (Fig. 1F), displaying a very significant reduction compared to the trimmed whisker condition (Fig. 1H; $P = 4.5 \times 10^{-5}$). This indicated, first, that BCs could not receive enough peripheral input to trigger c-Fos expression and, second, that no other brain areas (e.g., primary motor cortex) could do it either. Last, we injected lidocaine unilaterally and measured c-Fos$^+$ nuclei density in the BC contralateral to the injected side, which was deprived of direct thalamocortical input (input-blocked BC′; Fig. 1G; n_{hem} = 4, one hemisphere per mouse). Density was higher in the input-blocked BC′ than in BC sensory deprived through bilateral lidocaine injections (Fig. 1H; P = 0.0162). This suggested that the opposite, input-receiving BC triggered activity in the input-blocked BC′ through the callosal innervation. To confirm a callosal activation, we checked for anatomical overlap between c-Fos density and callosal fibers; hence, we normalized the density and assigned it to the different whiskers rows. Whereas density was homogeneously distributed across rows in the input-receiving BC (P = 0.5625), we found that was unevenly distributed in the input-blocked BC′ (P = 0.0021), where it concentrated in the CC-recipient posterolateral aspect (i.e., row A- and, to a lesser extent, row B-barrels; Fig. 1I). In input-blocked BC′, CC-recipient septa also showed a strong yet nonsignificant trend of higher posterolateral c-Fos density (Fig. 1J; P = 0.0507). These results demonstrate that, during novel object exploration, the posterolateral aspect of the BC′ is the main recipient of the activity raised by ipsilateral whiskers, which is likely recruited by the callosal pathway.

Strength and laminar pattern of postsynaptic activation differs between contra- and ipsilateral whisker responses

Since the posterolateral BC (plBC) subregion receiving high callosal innervation remained active despite the unilateral block of whiskers input, while less innervated areas were accordingly less active (Fig. 1, F and H), we characterized the corresponding contra- and ipsilateral whisker responses. To observe whisker responses in the areas of interest, we performed in vivo whole-cell patch-clamp recordings in anesthetized mice. Craniotomies were made following coordinates in *28*, targeting the representation of row A and row E barrel hollows and sides (Fig. 2, A and C), representing the whiskers nearest and farthest from the facial midline, respectively. Before whole-cell recordings, we performed a whiskers-to-barrels mapping by recording local field potential (LFP) responses upon contralateral whisker stimulation matching the target cortical representation (fig. S8C), here referred to as somatotopic stimulation. To further assess the targeting of selected areas, electrode tracks and recorded neurons were anatomically localized by biocytin-streptavidin staining in the corresponding brain sections (Fig. 2B). Considering that few unrecovered neurons were also included in the analysis, we refer to the row A–containing area as plBC and to the row E-containing area as the anteromedial BC (amBC). Groups of whiskers (either A_2-A_3 or E_2-E_3) were stimulated with a custom-made, solenoid-based whisker puller inspired by the study of Krupa *et al. 29* (fig. S8, A and B). Stimulations consisted of a firm caudo-rostro displacement [force: 7.4 ± 1.8 mN (mean ± SD); travel: 3.5 mm; duration: 15 ms] of the whiskers glued to the tip of a stainless-steel ultrafine wire, sliding backward upon solenoid electrification (fig. S8B). Once a cell was patched, somatotopic contra- and ipsilateral stimulations were delivered every 3 or 5 s (Fig. 2, A and B). Under anesthesia, the membrane potential (V_m) of cortical neurons oscillates periodically at ~1 Hz, alternating between up- and down-states (Fig. 2C). Because these spontaneous network transitions have a strong impact on whisker responses (fig. S2) (*30*, *31*), we analyzed separately stimulations/responses falling in either up- or down-state in 18 L2/3 neurons, 15 L4 neurons, and 37 L5/6 neurons.

First, we compared between ipsi- and contralateral evoked responses during down-state for all recorded neurons. Ipsilateral stimulations evoked responses characterized by longer onset delays [(ms): contra. = 12.3 (9.1 to 14.3), ipsi. = 18.6 (15.4 to 23.5), $P = 2 \times 10^{-5}$], weaker amplitude [(mV): contra. = 20.2 (16.9 to 26.8), ipsi. = 15.9 (11.6 to 21.9), $P = 5 \times 10^{-15}$], and lower probability to evoke action potentials compared to their contralateral counterparts [P(AP): contra. = 0.67 (0.2 to 1), ipsi. = 0.16 (0.04 to 0.5), $P = 5 \times 10^{-4}$].

Then, we studied how neurons of different layers responded to contra- and ipsilateral whisker deflections. Contralateral displacement of the whiskers robustly evoked responses, with the thalamorecipient L4 [10.7 (9.2 to 11.4) ms] showing the fastest onset delay, followed by L2/3 [12.6 (11.1 to 14.5) ms] and L5/6 [13.1 (8.8 to 14.7) ms] [Kruskal-Wallis (KW): df = 2, χ^2 = 6.44, P = 0.040]. In the same neurons, ipsilateral stimulation evoked responses in which onset delay of L5/6 tended to precede upper ones in a nearly significant fashion [L5/6: 16.5 (14.5 to 21.4) ms, L4: 19.6 (15.6 to 24.1) ms, L2/3: 19.6 (16.6 to 32.7); KW: df = 2, χ^2 = 4.792, P = 0.091]. If recording depth was considered instead of laminar identity, there was a significant inverse correlation with onset delay, with deeper neurons responding faster than upper ones (Pearson′s pairwise correlation: r = 0.36, P = 0.0018). Consistent with other descriptions (*6*, *12*, *14*–*16*), these data indicate that longer delay, lower amplitude, reduced spiking, and a different pattern of columnar activation distinguish S1 ipsilateral responses from contralateral ones.

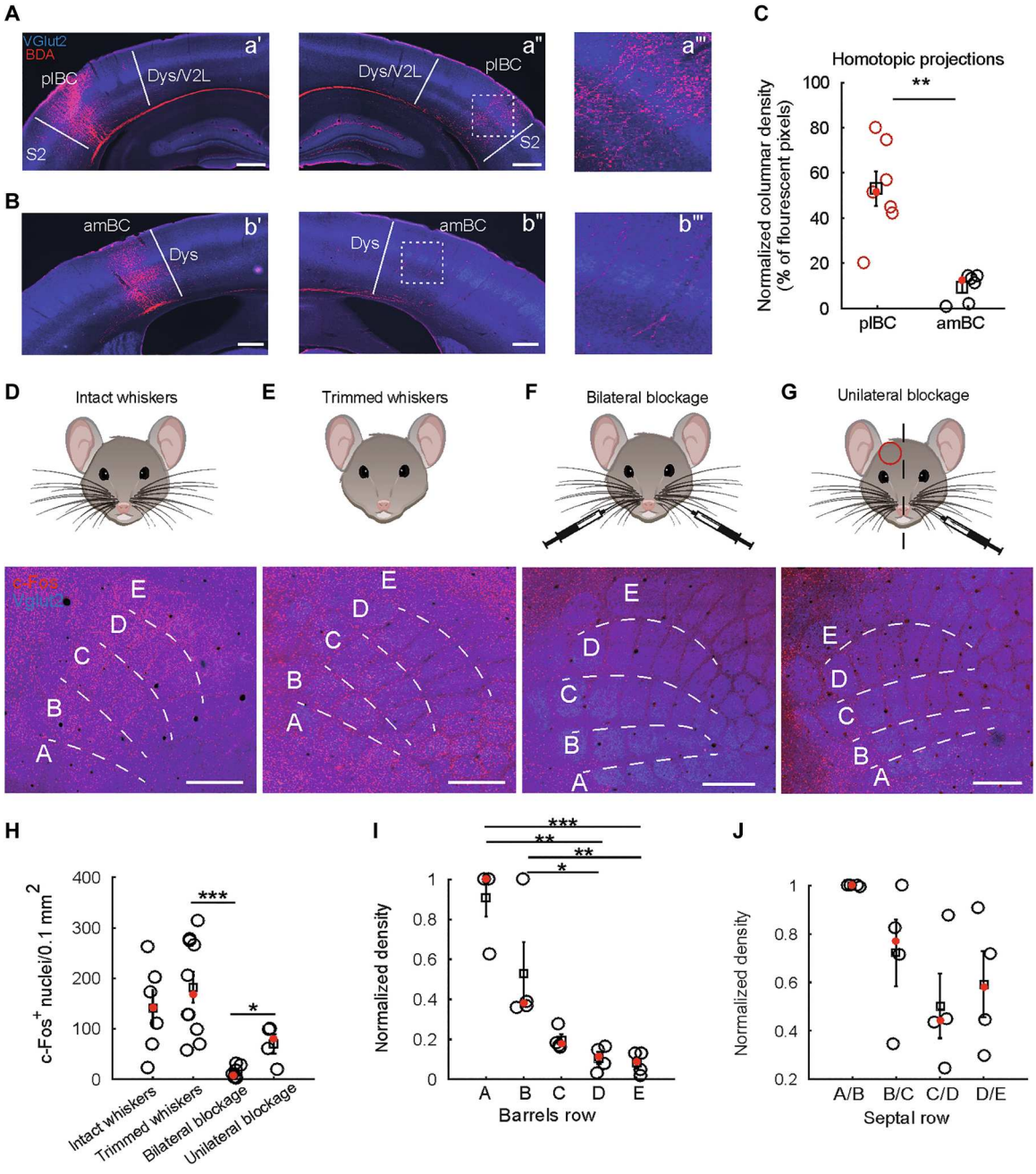

Fig. 1. Callosal innervation and the recruitment of c-Fos expression. (**A**) BDA injection in plBC (a′) with contralateral callosal innervation of the homotopic plBC (a″). a‴ shows inset from dashed square in a″. (**B**) BDA injection in amBC (b′) with contralateral callosal innervation of the homotopic amBC (b″). b‴ shows inset from b″. (**C**) Quantification of homotopic projections. (**D**) Mice carrying bilaterally intact arrays of whiskers. (**E**) Bilaterally trimmed whiskers mice. BC expresses c-Fos despite the peripheral intervention. (**F**) Bilateral input block through injections of lidocaine in the whisker pads nearly abolishes c-Fos expression in BCs. (**G**) Expression regionalizes toward row A- and B-whiskers upon input blockage of the contralateral whisker pad. Red circle indicates the side of input-blocked BC′. Images obtained by Z-projection across the tissue depth of maximal intensity for both channels. (**H**) Statistical comparisons of the density of c-Fos$^+$ nuclei across conditions. (**I**) Comparison of c-Fos expression across barrel rows normalized by the maximum density in each experiment (n = 4; KW density input-receiving BC: df = 4, χ^2 = 2.97, P = 0.5625; KW density input-blocked BC′: df = 4, χ^2 = 16.86, P = 0.0021; Fisher's least square difference (LSD) post hoc density input-blocked BC′: $P_{A\ versus\ B}$ = 0.5093; $P_{A\ versus\ C}$ = 0.0673; $P_{A\ versus\ D}$ = 0.0030; $P_{A\ versus\ E}$ = 7 × 10^{-4}; $P_{B\ versus\ C}$ = 0.2421; $P_{B\ versus\ D}$ = 0.0209; $P_{B\ versus\ E}$ = 0.0063; $P_{C\ versus\ D}$ = 0.2544; $P_{C\ versus\ E}$ = 0.1188; $P_{D\ versus\ E}$ = 0.6746). (**J**) Same as (I) for septa between barrel rows (n = 4; KW density input-blocked BC′: df = 3, χ^2 = 7.79, P = 0.0507). Dys, dysgranular area; Dys/V2L, dysgranular area/secondary visual cortex; S2, secondary somatosensory cortex. Scale bars, 500 μm (A and B) and 400 μm (D to G).

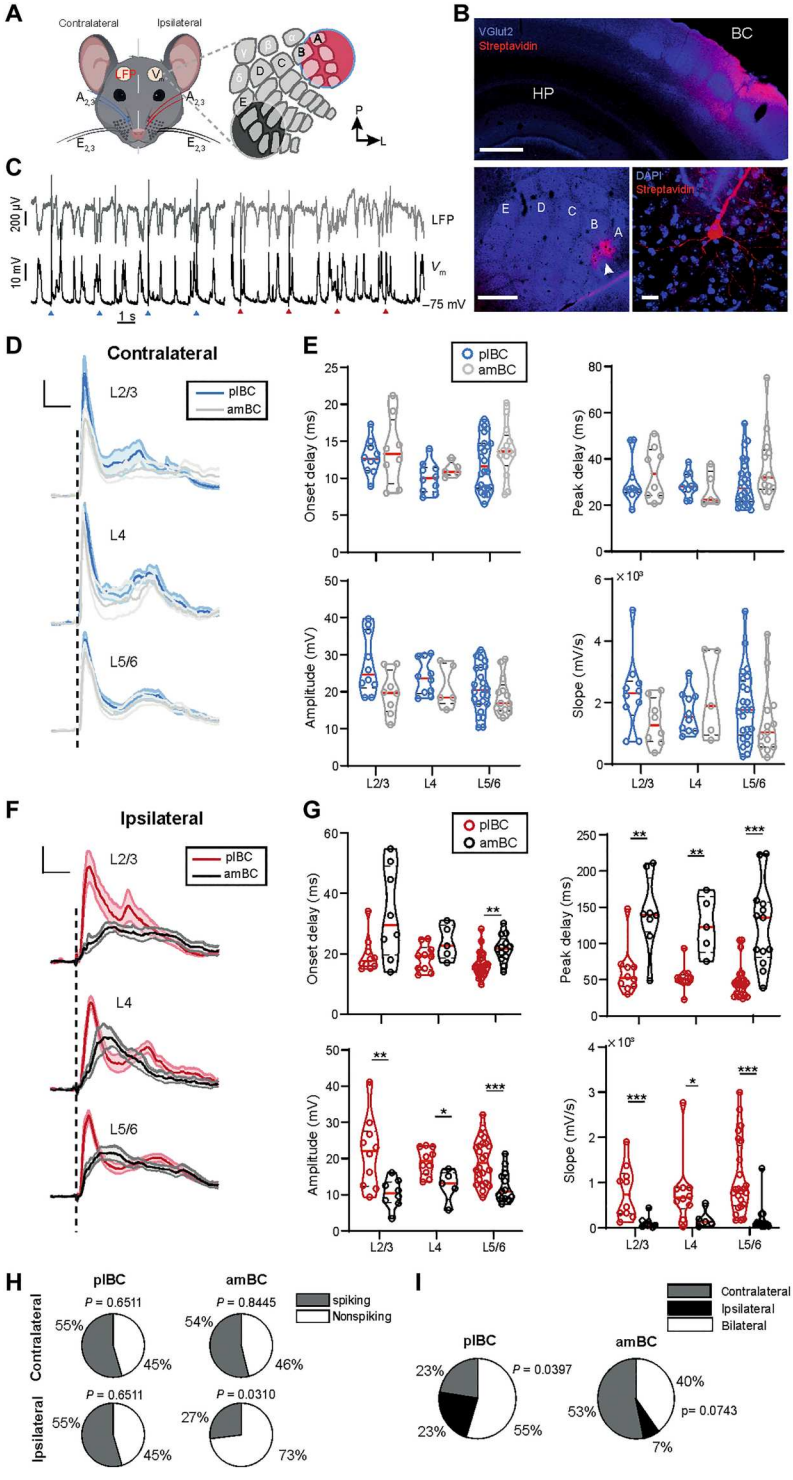

Fig. 2. Ipsilateral whisker responses are more vigorous in the plBC. (**A**) Cartoon of sides and sets of stimulated whiskers, color-coded according to the cortical subregion recorded, shown on the right. (**B**) Immunohistochemistry for assessing the placement of the whole-cell patch-clamp recording and cell anatomy. Top image: Example coronal section of a plBC recording site with biocytin-streptavidin staining. Scale bar, 400 µm. HP, hippocampus. Bottom images: On the left, example flatten brain preparation of L4 with biocytin-streptavidin staining within the row A representation (white arrowhead). Scale bar, 400 µm. On the right, example of a recovered pyramidal neuron with biocytin-streptavidin staining (red) and Vglut2 staining (blue). Scale bar, 20 µm. (**C**) Example of recordings in the plBC with whisker stimulation. Blue and red arrowheads for contra- and ipsilateral stimulations, respectively. (**D**) Grand average response ± SEM (shadows) following somatotopic contralateral stimulations along the cortical depth, aligned at stimulus delivery time (dashed line). Vertical bar = 5 mV, horizontal bar = 100 ms. (**E**) Statistical comparison of parameters of responses in (D). (**F**) Same as (D) for the same pool of neurons responding to somatotopic ipsilateral stimulations. Vertical bar = 5 mV, horizontal bar = 100 ms. (**G**) Statistical comparison of parameters of responses in (F). (**H**) Proportions of spiking and nonspiking neurons in the four conditions of stimulation/recording (for df = 1 in contralateral, plBC: 24/44, $\chi^2 = 0.2045$; amBC: 14/26, $\chi^2 = 0.0385$; for df = 1 in ipsilateral, plBC: 24/44, $\chi^2 = 0.2045$; amBC = 7/26, $\chi^2 = 4.6538$). (**I**) Distribution of suprathreshold RFs in spike-responding neurons (for df = 2, plBC: $\chi^2 = 6.4516$; amBC: $\chi^2 = 5.2000$).

Ipsilateral responses are stronger in the plBC

Next, to relate ipsilateral responses to distinct callosal innervation patterns, we compared neurons recorded in plBC (n = 44) and amBC (n = 26) in the different layers. Contralateral responses, except L2/3 neurons that tended to show higher amplitude in plBC than amBC (only significant during up-state: fig. S2, B to D; and in the multiunit activity: fig. S4C), did not differ in strength and temporal profile across layers (Fig. 2, D and E; fig. S3, A and B; and table S2). By contrast, ipsilateral responses markedly differed in these aspects between the same plBC and amBC neurons. In all layers, responses were stronger in plBC than in amBC neurons, with L5/6 response onset significantly faster in plBC than in amBC ones (Fig. 2, F and G; fig. S3, A and B; and table S2). In addition, during up-state, ipsilateral stimulation elicited responses in

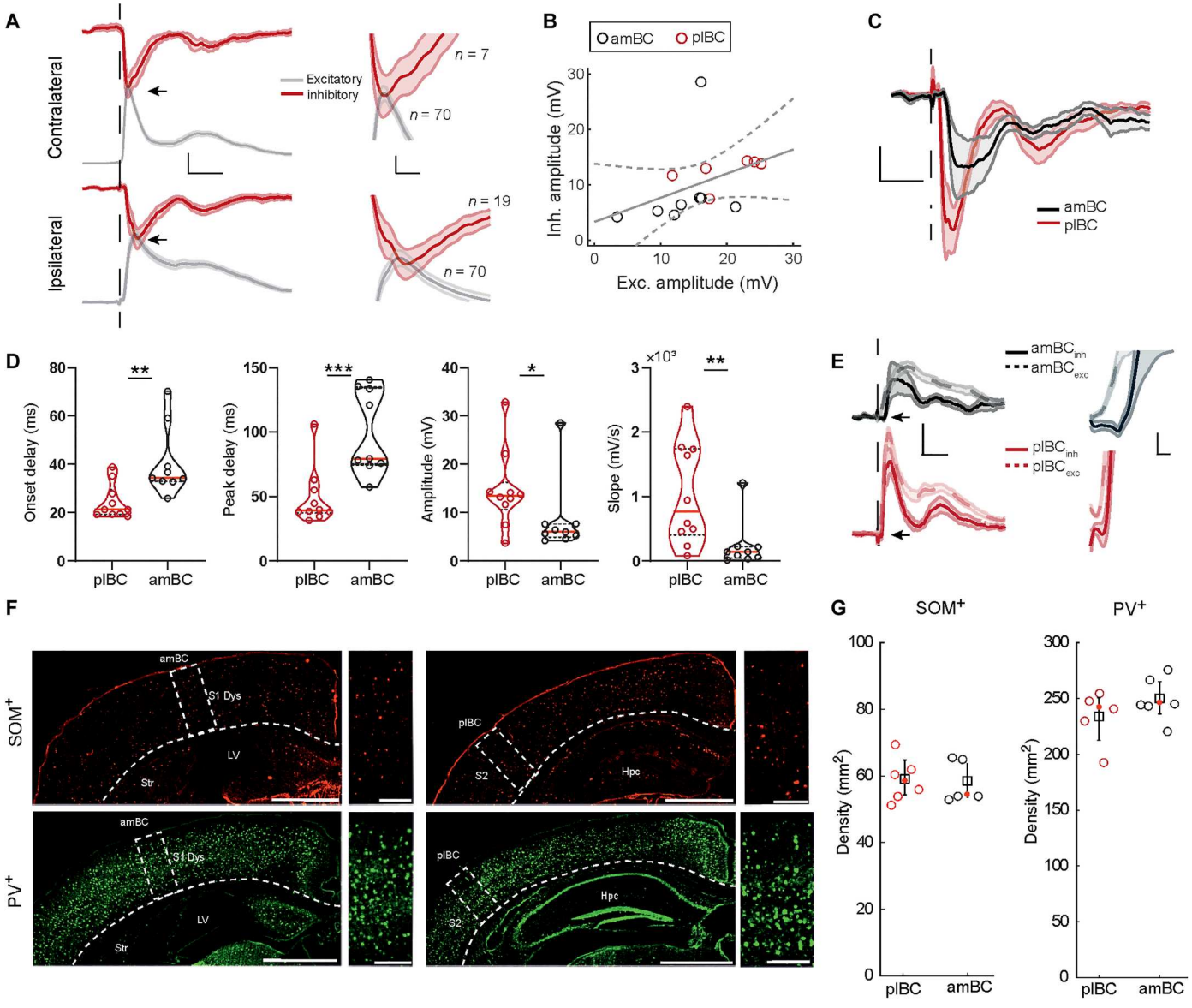

Fig. 3. Ipsilateral whisker stimulation recruits feed-forward inhibition. (**A**) Left: Grand average ± SEM (shadow) of excitatory (gray) and inhibitory (red) responses aligned at stimulus delivery time (dashed line). Vertical bar = 5 mV, horizontal bar = 100 ms. Right: Insets (black arrows) showing the nearly coincident peak between excitation and inhibition in both contra- and ipsilateral responses. Vertical bar = 2 mV, horizontal bar = 10 ms. (**B**) Inhibitory amplitude as a function of excitatory amplitude in response to somatotopic whisker stimulation in the same neurons [correlation (Spearman), all neurons considered together: rho = 0.62, $P = 0.0202$]. (**C**) Grand average ± SEM (shadow) of inhibitory responses aligned at stimulus delivery time (dashed line) recorded in the two subregions. Vertical bar = 5 mV, horizontal bar = 100 ms. (**D**) Statistical comparison of parameters for responses in (C). (**E**) Left: Excitatory (dashed line) and inhibitory (solid line) grand averages ± SEM (shadow) in the two BC subregions aligned at stimulus delivery time (vertical dashed line), with inhibitory responses inverted in sign with respect to (C) for visualization. Vertical bar = 5 mV, horizontal bar = 100 ms. Right: Insets from black arrows on the left showing the grand average around the onset of the excitatory and inhibitory components. Vertical bar = 1 mV, horizontal bar = 10 ms. (**F**) Examples of SOM^+ (red) and PV^+ (green) immunostaining. Insets magnify the amBC (left) and plBC (right) quantified subregions, indicated by the dashed line rectangles, horizontal bars = 0.5 mm. (**G**) Statistical comparisons of stained interneurons in plBC (red circles) and amBC (black circles) for SOM^+ (left, $P = 0.63$) and PV^+ (right, $P = 0.75$).

the majority of plBC neurons but rarely in amBC neurons (fig. S2, C and D). Following contralateral stimulation, about half of the neurons in both plBC and amBC responded with spiking activity; while for ipsilateral stimulation, this fraction was much smaller in amBC but not in plBC (Fig. 2H), suggesting an increased ipsilateral output in the latter. We also analyzed the laminar distribution of spike-responding neurons (fig. S2A). Following contralateral stimulation, spike-responding neurons were evenly dispersed throughout layers in both plBC and amBC; following ipsilateral stimulation, this pattern was statistically preserved in amBC, yet spike-responding neurons were significantly concentrated in L5/6 in plBC (15 of 24; df = 2, $\chi^2 = 9.25$, $P = 0.0098$; fig. S3C), suggesting downstream targets being preferentially subcortical or interhemispheric. Considered across layers, suprathreshold RFs (Fig. 2I) in

plBC were most commonly bilateral (17 of 31, 54%), with remaining neurons equally split between contra- (7 of 31, 23%) and ipsilateral RFs (7 of 31, 23%). Ipsilateral suprathreshold RFs were almost absent in amBC (1 of 15, 7%), with a nearly significant tendency for contralateral RFs to be the most represented class (8 of 15, 53%), followed by the bilateral one (6 of 15, 40%). Hence, while the plBC seems to equally represent both the ipsi- and contralateral sensory hemispaces, the amBC is mostly dedicated to the contralateral one. In a set of experiments with silicon probe electrodes (n = 8 mice), multiunit activity was obtained along the cortical columns in amBC and plBC subregions responding to ipsi- and contralateral stimulation (fig. S4). Consistent with a marked ipsilateral representation, the spike ratio between ipsi- and contralateral responses was higher in plBC than in amBC. Moreover, the peak delay measured at the maximum of the spiking response for ipsilateral stimulation was shorter in plBC than in amBC (fig. S4C).

The greater ipsilateral sensitivity of plBC neurons compared to amBC neurons could not be attributed to different intrinsic excitability, since their electrophysiological membrane properties were not different in either up- or down-states (table S3), instead suggesting a distinct synaptic recruitment. Overall, these results demonstrate that the plBC is populated by neurons endowed with a RF highly sensitive to the stimulation of ipsilateral (row A) whiskers, likely due to stronger callosal inputs.

Ipsilateral responses are controlled by feed-forward inhibition

In the BC, feed-forward inhibition is best known to act at thalamocortical synapses through a disynaptic mechanism mediated by parvalbumin-positive (PV^+) or somatostatin-positive (SOM^+) GABAergic interneurons (*32*, *33*). This type of inhibition can modulate the time window for thalamic input integration (*34*) and be governed by the direction of whisker deflections (*35*). Like thalamocortical afferents, callosal afferents can also mediate disynaptic feed-forward inhibition in distinct neocortical areas of rodents (*36*–*38*) and cats (*3*). Yet, despite the presence of direct callosal contacts on inhibitory interneurons (*39*) and the increased firing of putative fast-spiking neurons upon ipsilateral stimulation (*16*), to our knowledge, no study so far has directly demonstrated the presence of inhibitory ipsilateral responses elicited by feed-forward inhibition in the mouse S1. To address that, and to decompose the excitatory and inhibitory response components, we used a low-chloride intracellular solution (see Materials and Methods), enabling us to hold recorded neurons at the reversal potential for excitation (~−5 mV) or GABAa inhibition (~−70 mV). By injecting positive currents to depolarize neurons close to their excitatory reversal potential, we sampled inhibitory responses to contra- (n = 7) and ipsilateral (n = 19) somatotopic whisker stimulation.

As expected, contralateral stimulations could reliably evoke inhibitory responses (Fig. 3A), whose peak delay was nearly coincident with the excitatory one of the entire neuronal pool [contra. peak delay (ms): E = 27.8 (24.2 to 37.8), n = 70, I = 30.2 (29.2 to 36.7), n = 7, P = 0.2568]. Comparable to their contralateral counterparts, ipsilateral stimulations also elicited responses with the excitatory and inhibitory components (Fig. 3, A and B). The amplitude of inhibitory and excitatory ipsilateral responses showed a significant lineal relation when both were recorded in the same neurons (n = 14; Fig. 3B), with inhibitory response amplitude being comparatively smaller. To observe whether ipsilateral inhibitory responses could vary similarly to the excitatory ones following the extent of local callosal innervation (Fig. 1, A and B), we compared plBC neurons (n = 10) with amBC ones (n = 9) (Fig. 3C). As with the excitatory component, inhibition was faster and much more vigorous in plBC than in amBC (Fig. 3D and table S4), suggesting that the inhibitory responses also relied on callosal innervation. Furthermore, both the excitatory and inhibitory components seemed to show different temporal dynamics between the two subregions. Therefore, we compared the onset and peak delay separately for plBC and amBC. In both subregions, the onset of inhibitory responses was significantly delayed with respect to excitatory responses, consistent with a feed-forward inhibition mechanism. Yet, this was accompanied by regional differences underlying the onset of the inhibitory component. Specifically, in plBC, the inhibitory component was delayed only by ~5 ms compared to the excitatory one (medians′ difference), while in amBC by ~12 ms [Fig. 3, D and E; onset (ms): plBC: E = 16.4 (14.8 to 19.5), I = 21.3 (19.3 to 27.8), P = 0.0010; amBC: E = 22.5 (19.1 to 28.1), I = 34.3 (32.9 to 44.1), P = 0.0008]. Dissimilar postsynaptic inhibitory circuits could underlie the earlier and stronger inhibitory responses observed in plBC. To explore this possibility, we compared the number of PV^+ and SOM^+ interneurons located in amBC and plBC, labeled by immunostaining (see Materials and Methods). We found similar proportions of PV^+ and SOM^+ interneurons in both territories (Fig. 3, F and G), suggesting similar components in postsynaptic inhibitory circuits in both BC subregions.

Ipsilateral responses in the plBC have their origin in the contralateral hemisphere

What is the source of the vigorous ipsilateral response? While normally described as totally decussating toward the contralateral somatosensory thalamus (*14*), principal sensory nucleus (PrV) axons branch extensively (*40*), and some of them, emanating from its dorsal portion, reach the ipsilateral thalamus (*41*). The dorsal PrV represents midline body parts such as the lower jaw and lips (*42*), with the representation of the former also receiving CC afferents at the cortical level (*43*). Although row A-whiskers are represented in the ventral PrV, they lie next to the facial midline and cortically receive CC afferents. Thus, we could not exclude a priori that few ipsilateral trigeminothalamic axons, or an earlier commissure, could have passed undetected so far and be responsible for the vigorous ipsilateral response in plBC. To exclude these possibilities and learn about the contribution of callosal neurons to the sensory response, we injected tetrodotoxin (TTX; 1 to 1.5 μl, 100 μM) in one BC while recording in the opposite plBC (n = 11, one neuron per mouse) (Fig. 4A). Contra- and ipsilateral row A-whiskers were stimulated before [control (CTRL) and after (TTX)] the drug application, keeping the neuron under whole-cell patch-clamp. Amplitude of LFP downward deflections in the injected BC greatly decreased upon TTX application (Fig. 4, A and C), indicating a strong depression of its excitatory activity. In the opposite hemisphere, although a weak depolarization could still be evoked, the response to ipsilateral row A-whisker stimulation lost its timing and vigor (Fig. 4, D and E, and fig. S5, A and B). This suggests a weaker synaptic recruitment in TTX compared to CTRL, demonstrating a strong dependence of the ipsilateral response on callosal neurons of the opposite BC. We also measured spiking activity by analyzing multiunit recordings; plBC responses decreased to 75% on average after TTX (Fig. 4, F to H).Yet, the persistence of a

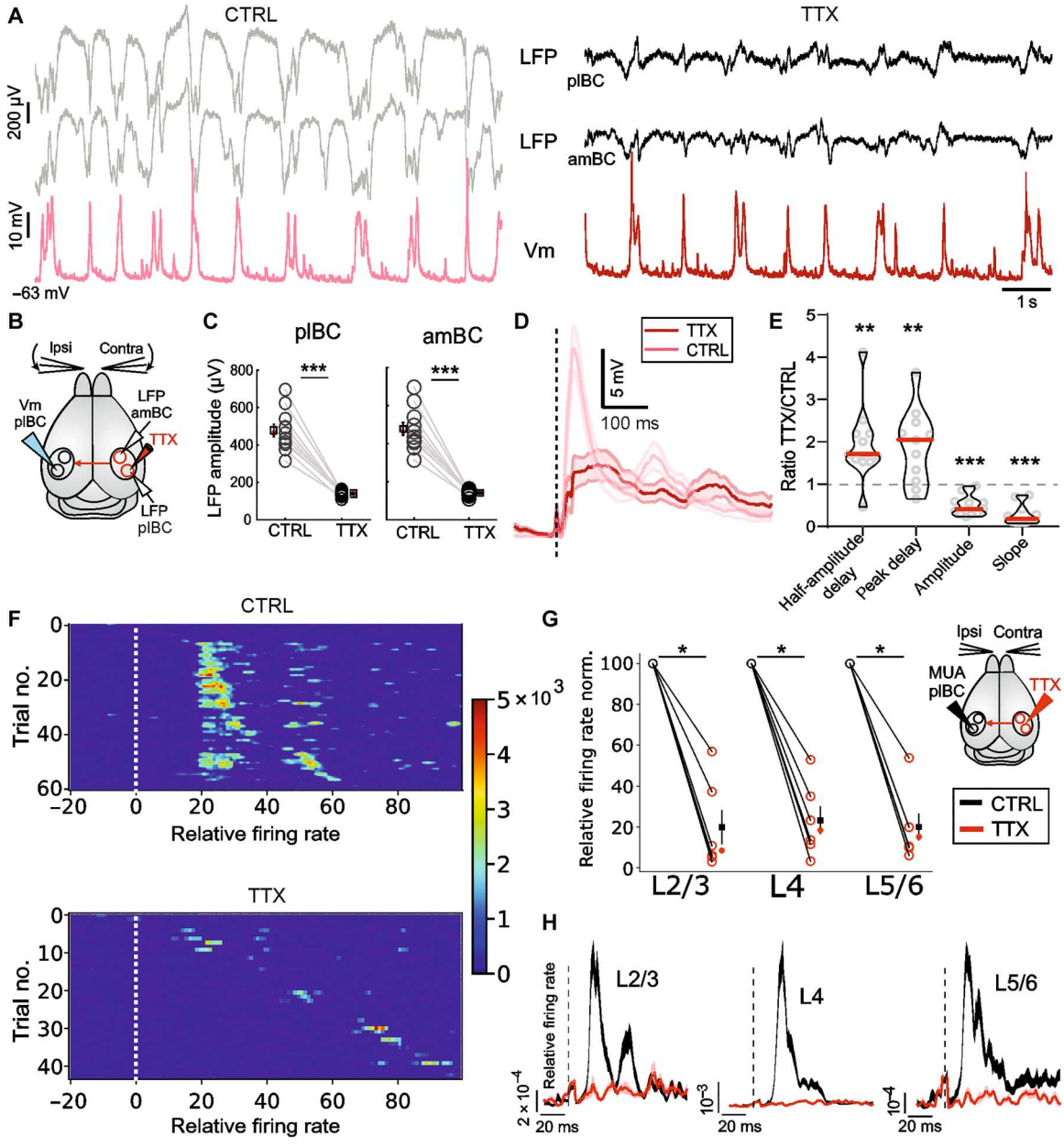

Fig. 4. Synaptic recruitment deteriorates upon activity blockage of the opposite BC. (**A**) Example recording of a plBC neuron (red bottom trace) and contralateral plBC and amBC LFPs (left, gray traces) during spontaneous activity. Note the activity suppression of the contralateral BC, at both plBC and amBC locations, upon TTX application (right, black traces). (**B**) Diagram of the experiment; S1 of both cortical hemispheres with amBC and plBC (circles), in red TTX injection. (**C**) Statistical comparison of LFP downward deflections' amplitude between CTRL and TTX [plBC amplitude (µV): LFP_{CTRL} = 463.0 (408.4 to 528.1), LFP_{TTX} = 141.4 (130.7 to 152.6), Wilcoxon signed-rank (WSR): $P = 9.7 \times 10^{-4}$; amBC amplitude (µV): LFP_{CTRL} = 418.0 (335.0 to 515.8), LFP_{TTX} = 148.9 (137.9 to 171.3), WSR: $P = 8.5 \times 10^{-5}$]. (**D**) Grand average ± SEM (shadow) of row A-whiskers responses aligned at stimulus (dashed line). (**E**) Averages of parameters of responses in c [WSR: onset delay (ms): CTRL = 18.6 (15.7 to 19.4), TTX = 21.3 (18.7 to 22.8), $P = 0.0313$; peak delay (ms): CTRL = 46.2 (42.8 to 49.1), TTX = 94.5 (42.2 to 109.9), $P = 0.0137$; amplitude (mV): CTRL = 21.1 (12 to 23.3), TTX = 8.3 (6.4 to 10.1), $P = 0.0010$; slope (mV/s): CTRL = 865 (538 to 985), TTX = 178 (67.1 to 320), $P = 0.0010$]. (**F**) Raster plots of relative firing rate centered around the onset of the stimulation for a representative electrode of plBC in response to ipsilateral stimulation before (upper) and after (bottom) TTX. (**G**) Effect of TTX in the relative firing rate of the different layers of plBC responding to ipsilateral stimulation [supragranular: CTRL = 4.1×10^{-3} (2.56×10^{-3} to 5.06×10^{-3}), TTX = 1×10^{-3} (1.7×10^{-4} to 9.8×10^{-4}), P = 0.0315; granular: CTRL = 1.9×10^{-3} (1.18×10^{-3} to 1.8×10^{-3}), TTX = 6.3×10^{-4} (1.7×10^{-4} to 5.5×10^{-4}), P = 0.0315; infragranular: CTRL = 1.4×10^{-3} (6.6×10^{-4} to 1.7×10^{-3}), TTX = 4.6×10^{-4} (8.8×10^{-5} to 2.1×10^{-4}), P = 0.0315]. Right inset: Diagram of the experiment. (**H**) Representative examples of the average relative firing rate peristimulus time histogram in the supragranular (left), granular (middle), and infragranular (right) layers of plBC before (black) and after (red) TTX release in the contralateral BC, responding to the ipsilateral stimulation (dashed line).

weak evoked response after contralateral TTX blockage required a further validation of the callosal scenario. If the CC was driving these responses, then directly stimulating the opposite BC should have evoked responses reflecting the difference in callosal innervation between plBC and amBC (Fig. 1, A to C), similar to the sensory ones evoked from the whiskers (Fig. 2F). In this case, the residual response observed in TTX would be accounted for by an incomplete activity suppression of the drug-receiving hemisphere. To explore this issue, we took advantage of *NEX-Cre* mice that allow the genetic targeting of cortical projection neurons (*44*). We injected a Cre-dependent adeno-associated viral vectors expressing channelrhodopsin-2 (AAV-ChR2) carrying enhanced yellow fluorescent protein (EYFP) in the BC to impose its excitation by blue-light illumination (5- or 10-ms light step) while recording neurons in the opposite plBC ($n = 11$) or amBC ($n = 12$). To be sure about restricting the activation of only homotopic contralateral areas, for most of the recorded neurons (20 of 23), two LFPs were collected in amBC and plBC of the illuminated hemisphere, with the optic fiber positioned over one of the two, in mirror-symmetric (i.e., homotopic) opposition to the contralateral patch-clamp electrode (Fig. 5, A and B).

Again, the great majority of EYFP-positive callosal axons invaded the BC at the S1/S2 border (Fig. 5, C and D), enveloping the row A-whiskers representation with scanter labeling of the septa (Fig. 5C). Upon blue-light illumination, the mirror symmetric LFP activated locally and powerfully (Fig. 5, E and F). Clearly reflecting a more vigorous input from the opposite hemisphere, optogenetic responses of plBC neurons had much higher amplitudes and steeper slopes than those of amBC, while the remaining parameters were similar (Fig. 5, G and H). As expected, the overall difference in shape between amBC and plBC responses recapitulated with fidelity the difference in dynamics between the ipsilateral whiskers' responses. Statistically comparing the waveforms between plBC and amBC neurons evoked by optogenetic and sensory stimulations resulted in a similar pattern of significant (and nonsignificant) *P* values over time (Fig. 5I). In addition, in neurons receiving both the ipsilateral whiskers and interhemispheric optogenetic stimulations (Fig. 5J; plBC $n = 4$, amBC $n = 6$), cross-correlation between waveforms of the two evoked responses was extremely high in both subregions (~0.90; Fig. 5K), likely reflecting the shared recruitment of CC fibers across stimulation types. These results strongly suggest that the callosal input alone underlies the different ipsilateral responses between plBC and amBC neurons.

Ipsilateral responses mimic their contralateral counterparts in the plBC

Given the proximity to the facial midline of row A-whiskers, the callosal afferents invading its cortical representation at the S1/S2 border, and the vigorous callosal response reminiscent of a thalamocortical one, we inspected the data looking for neurons able to respond comparably to contra- and ipsilateral row A-whisker stimulation, namely, side-invariant responding neurons (*6*). Notably, in the three-dimensional space individuated by the raw response parameters (i.e., peak delay, amplitude, and slope), the pool of ipsilateral responses tends to overlap with the contralateral one in plBC but not in amBC (fig. S6). To quantify the similarity between ipsi- and contralateral responses in the two BC subregions, parameters were normalized in the *z*-distribution, and the Mahalanobis distance was measured for each response type (Fig. 6, A and B). We found that the distance of ipsi- from contralateral excitatory responses (Fig. 6C) was much shorter in plBC than amBC neurons ($P = 1.2 \times 10^{-6}$). An analogous result was obtained for inhibitory responses (Fig. 6C) when pooled contralateral ($n = 7$) and separated ipsilateral responses from plBC and amBC were compared ($P = 9.7 \times 10^{-4}$), extending this contra-/ipsilateral similarity up to the pattern of inhibition. Cross-correlation was also higher between contra- and ipsilateral excitatory responses recorded in plBC than in amBC, while both measures dropped under TTX in plBC (Fig. 6D), confirming a role for the CC in producing the similarity between the two responses. Last, in more than one third of plBC neurons (34%, 15 of 44), the cross-correlation between contra- and ipsilateral responses exceeded 0.95, while in amBC, it was only 3.8% (1 of 26) (Fig. 6D). Such plBC neurons were unevenly distributed along the cortical depth, with the majority concentrated in L5/6 (Fig. 6F) and showing an ipsilateral response indistinguishable from the contralateral one (Fig. 6E). Notably, their rate and probability of action potential firing were also statistically equivalent, in contrast with remaining plBC neurons that were more sensitive to the contralateral side (Fig. 6, G and H). These data demonstrate the presence of row A side-invariant responding neurons restricted to the plBC and suggest their involvement in the representation of the midline of the whiskers' sensory space.

The posterolateral region receives heterotopic contralateral synaptic inputs more robustly than the anteromedial one

While showing a preference for a given whisker, BC neurons can also respond to the stimulation of whiskers other than the preferred one (*45*, *46*). Critically, integrating whisker inputs across the whisker array allows BC neurons to represent complex features of objects in the somatosensory space (*47*, *48*). To represent the right and left whiskers' sensory hemispaces in unison, such an operation may be required across the hemispheres (*7*). The presence of callosal heterotopic connectivity would allow the interaction between nonpreferred whisker representations of the two BCs. To explore this possibility, we analyzed the heterotopic projections of plBC and amBC after BDA injections. Our result showed a scant presence of heterotopic axons reaching the opposite hemisphere at nonmirror symmetric regions, respectively, in amBC and plBC (Fig. 7A), with a tendency to be slightly higher in plBC (Fig. 7B; $P = 0.073$). Next, we examined synaptic responses of callosal heterotopic connectivity. We expressed ChR2 in the BC of *NEX-Cre* mice and compared the evoked responses to the homotopic, heterotopic, or both simultaneously (BC_{wide}) light activation of the contralateral BC (Fig. 7, C to J). In addition to the recorded neurons, we also obtained extracellular LFP recordings in the stimulated BC to ensure the optogenetic activation pattern (Fig. 7, E and F). Notably, while 100% (four of four) of plBC neurons could respond to BC_{he} stimulation, a response was detected only in 57% (four of seven) of amBC neurons, suggesting that plBC neurons are more functionally connected with heterotopic contralateral territories than amBC ones. In amBC, BC_{he} stimulation evoked responses at longer onset delays than the BC_{ho} stimulation ($P = 0.0084$; Fig. 7, G and H, and table S5). By contrast, onset delays did not differ in plBC ($P = 0.2637$; Fig. 7, I and J). The high proportion of responding neurons and the absence of onset delays differences suggest that heterotopic CC fibers can activate plBC neurons as directly as the homotopic ones, while this activation is rarer and likely mediated by a more

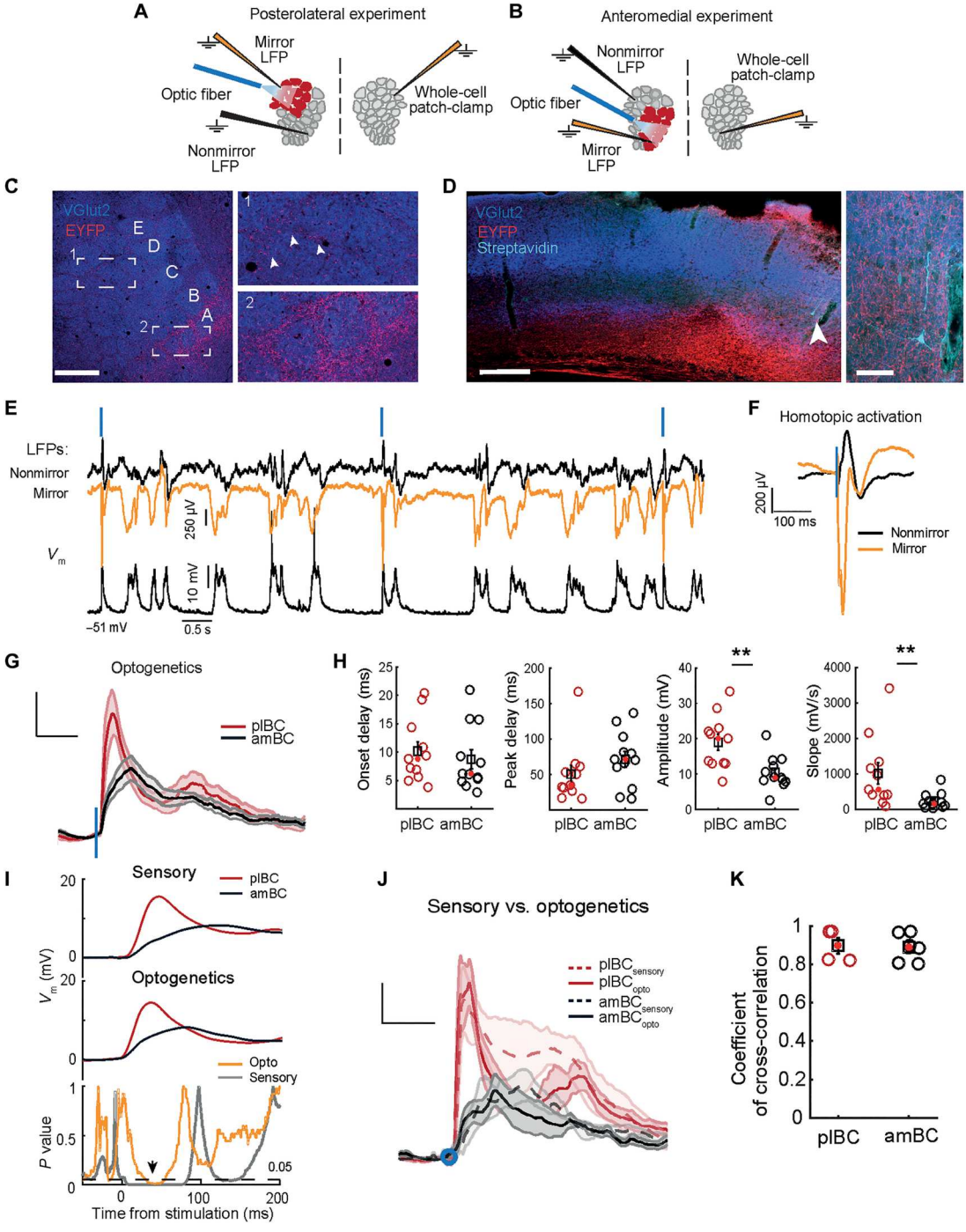

Fig. 5. Homotopic cortically evoked responses recapitulate sensory ones. (**A**) Experimental setting for homotopic optogenetic stimulation/recording in plBC. (**B**) Same as (A) for the amBC. (**C**) Flatten L4 preparation of the BC contralateral to the AVV-EYFP-ChR2–injected hemisphere of an example *Nex-Cre* mouse. Insets show scanter callosal innervation of septa (top) compared to row A representation (bottom). Scale bar, 500 µm. (**D**) Same animal preparation as (C) but in coronal section. Scale bar, 200 µm. Inset shows pyramidal neuron recorded within the bulk of invading callosal axons. Scale bar, 50 µm. (**E**) Example stimulation/recording of homotopic optogenetic experiment in plBC. (**F**) Example waveform averages of mirror and nonmirror LFPs in homotopic experiments aligned at stimulus delivery time (blue line). (**G**) Grand average ± SEM (shadow) of the whole-cell recordings with optogenetic responses aligned at stimulus delivery time (blue line). Vertical bar = 5 mV, horizontal bar = 100 ms. (**H**) Statistical comparison of parameters of responses in (G) [onset delay (ms): plBC = 8.8 (5.9 to 13.5), amBC = 6.1 (5.0 to 12.5), $P = 0.4060$; peak delay (ms): plBC = 34.9 (28.1 to 59.0), amBC = 71.1 (45.0 to 92.4), $P = 0.1029$; amplitude (mV): plBC = 20.1 (13.0 to 22.8), amBC = 9.0 (8.1 to 13.0), $P = 0.0089$; slope (mV/s): plBC = 561.4 (397.4 to 3×10^3), amBC = 152.1 (80.5 to 309.0), $P = 0.006$]. (**I**) Grand averages of sensory (top) and optogenetics (middle) responses and *P* value distributions (bottom) resulting from their comparison. Black arrowhead = region of overlap for $P < 0.05$. (**J**) Grand average ± SEM (shadow) of sensory and optogenetic responses recorded in the same neurons aligned at response onset (blue circle). Vertical bar = 5 mV, horizontal bar = 100 ms. (**K**) Cross-correlation between sensory and optogenetic responses of the neural populations in (J) [coeff.$_{sensory/opto}$: plBC ($n = 4$): 0.89 (0.82 to 0.97), amBC ($n = 6$): 0.89 (0.80 to 0.96)].

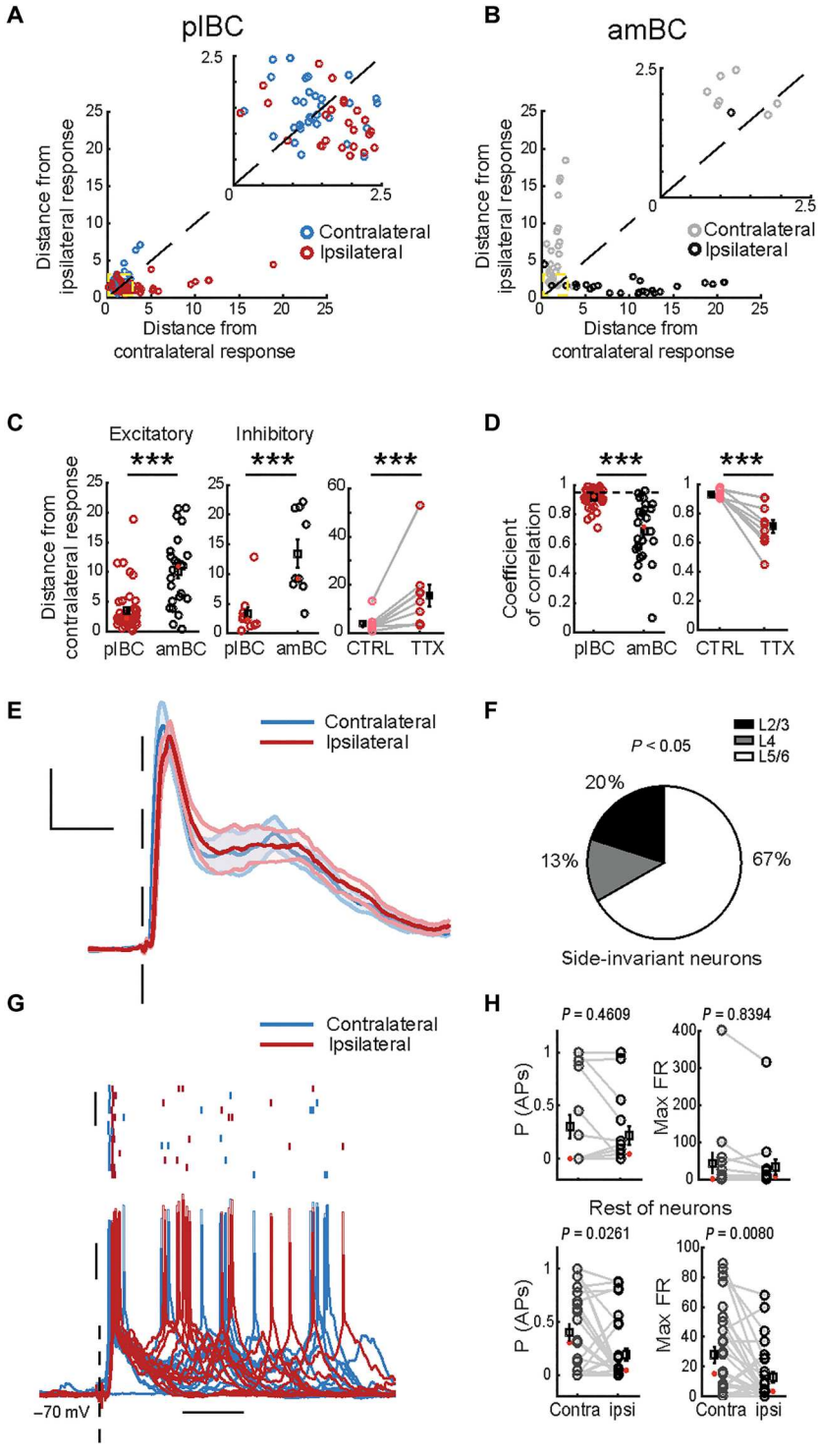

Fig. 6. Side-invariant representation of row A-whiskers. (**A**) Mahalanobis distance [arbitrary units (a.u.)] in plBC. Inset shows magnification within 2.5 a.u. in plBC (red and blue) and in amBC (black and gray). (**B**) Same as (C) in amBC. Color-code as (B). (**C**) Statistical comparisons of ipsi-to-contralateral distance [*x* axis in (C) and (D)] for the excitatory (left) and inhibitory (center) response components, plus the effect of TTX on the excitatory one (right) [excitatory (exc.) distance (a.u.): plBC = 2.2 (1.6 to 3.7), amBC = 11.0 (5.4 to 12.8), $P = 1.2 \times 10^{-6}$; inhibitory (inh.) distance (a.u.): plBC = 2.3(1.4 to 3.4), amBC = 9.2(8.1 to 21.1), $P = 9.7 \times 10^{-4}$; WSR test on $exc._{TTX}$ distance (a.u.): CTRL = 2.7(2.4 to 3.5), TTX = 14.8(3.9 to 17.0), $P = 0.0020$]. (**D**) Cross-correlation coefficients between contra- and ipsilateral waveform averages of single neurons (left) and the effect of TTX (right) [$coeff._{contra/ipsi}$: plBC = 0.92 (0.88 to 0.96), amBC = 0.71 (0.56 to 0.83), $P = 1.3 \times 10^{-7}$; WSR test on $coeff._{contra/ipsi}$ in TTX: CTRL = 0.92 (0.90 to 0.96), TTX = 0.70 (0.62 to 0.83), $P = 0.0020$]. Horizontal dashed line indicates 0.95. (**E**) Grand average ± SEM (shadows) of contra- and ipsilateral row A-whiskers responses aligned at stimulus delivery time (dashed line) with correlation in (F) > 0.95. Vertical bar = 5 mV, horizontal bar = 100 ms. (**F**) Side-invariant responding neurons in g preferentially occupy L5/6 [df = 2, $\chi^2 = 7.60$, $P < 0.05$]. (**G**) Example raw trace of a side-invariant spike-responding neuron (bottom) with rasterplot (top). Responses are aligned at stimulus delivery time (dashed line). Vertical bars = 5 trials (top), 10 mV (bottom); horizontal bar = 100 ms. (**H**) Quantification of firing activity following row A-whisker stimulations.

indirect pathway in amBC neurons. Nonetheless, responses to BC_{he} stimulation were generally weaker than the BC_{ho} and BC_{wide} stimulation in plBC neurons (Fig. 7, I and J): Amplitude and slope were reduced, and the maximal peak was delayed in this condition (table S6). Together, the anatomical and electrophysiological data show that the heterotopic innervation is weaker than homotopic innervation in plBC. Last, responses to BC_{wide} stimulation were slightly more vigorous than BC_{ho} stimulations (Fig. 7, G to J), suggesting a certain degree of input summation between homo- and heterotopic contralateral territories (Fig. 7, I and J). Yet, responses did not differ statistically, confirming that the two BCs mainly operate in a homotopic fashion with a small heterotopic contribution.

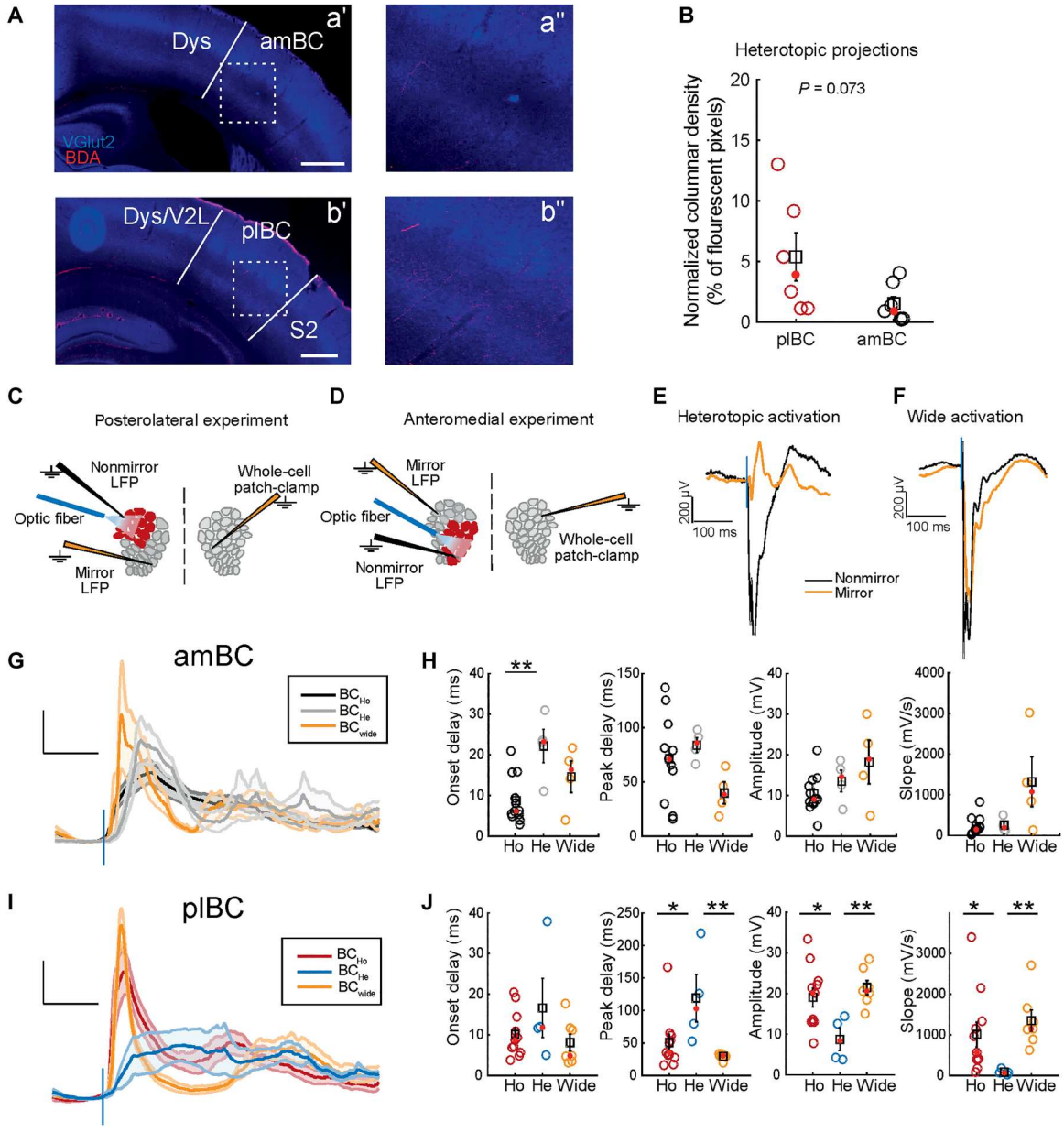

Fig. 7. Homotopic, heterotopic, and wide callosal activation of the BC subregions. (**A**) Heterotopic axons in amBC from contralateral plBC BDA injection (a′) with inset from dashed square (a″), top images. Heterotopic axons in plBC from contralateral amBC BDA injection (b′) with inset from dashed square (b″), bottom images, in both cases coronal slices. Note that contralateral BDA injections are from the same brains of Fig. 1 (A and B). (**B**) Statistical comparison of heterotopic axonal fluorescence in amBC and plBC. (**C**) Schema of the experimental setting for heterotopic optogenetic stimulation and recordings in plBC. (**D**) Same as (D) for amBC. (**E**) Example waveform averages of mirror and nonmirror LFPs in heterotopic experiments aligned at stimulus delivery time (blue line). (**F**) Same as (F) for wide activations of the BC. (**G**) Grand average ± SEM (shadows) of optogenetic responses aligned at stimulus delivery time (blue vertical line) in the three conditions in amBC. Note that homotopic response is the same shown in Fig. 5G. Vertical bar = 5 mV, horizontal bar = 100 ms. (**H**) Statistical comparison of parameters for responses in (H) [KW onset delay (ms): df = 2, $\chi^2 = 7.09$, $P = 0.0084$]. Fisher's LSD post hoc test values for (I) and (K) are provided in table S5. (**I**) Same as (H) in plBC. Vertical bar = 5 mV, horizontal bar = 100 ms. (**J**) Statistical comparison of parameters for responses in (J) [KW onset delay (ms): df = 2, $\chi^2 = 2.67$, $P = 0.2637$]. Scale bars, 500 µm (a′ and b′). Ho, homotopic; He, heterotopic.

DISCUSSION

Studies on the callosal contribution to BC activity (*11*–*16*, *49*) have so far disregarded how ipsilateral responses relate to the callosal innervation arrangement (*19*–*25*). To our knowledge, the only study in which whiskers of different rows were stimulated and ipsilateral responses were recorded did not include the stimulation of row A (*14*). Available data on this circuit are provided in *39*, where ex vivo monosynaptic callosal connections were mapped throughout the cortical depth in the row A representation. Yet, such a preparation did not allow recording of the associated sensory responses. Here, we show that the row A representation in plBC is the most active despite the block of thalamocortical inputs during mouse

exploratory behavior. Bilateral trimming of the whiskers was not enough to refrain the BC thalamocortical activation (Fig. 1E). Curiously, the anteroposterior extent of c-Fos expression differed between intact whiskers (A < P) and trimmed whiskers (A > P) cohorts (fig. S1, A and B). Unlike in the posterior aspect, in the anterior aspect of the BC, the representation of the furry skin intervening between whisker follicles overlaps with that of small, anterior whiskers (*50*). Together with our common observation that mice with bilaterally trimmed whiskers touched cage walls and littermates directly with the snout, these results could reflect a different exploration strategy. We hypothesize that, while mice with intact whiskers mostly used long whiskers during exploration, mice with trimmed whiskers used the common fur on the anterior snout, thereby activating the barrels representing short whiskers. Such an activation is not reported normally for mice left with only one whisker. Perhaps, the spared whisker allows mice to maintain a proper distance between snout and surfaces, an otherwise difficult task. Further, behavioral studies are needed to confirm this interpretation. Nevertheless, lidocaine injection in the whisker pads could prevent such activation and be used to isolate the ipsilateral contribution to the activity of BC subregions, which remarkably overlapped with the pattern of callosal innervation (Figs. 1, A and D to G, and 5A).

Neural pathways

Contralateral stimulations activated L4 faster than L2/3 and L5/6. This suggests the recruitment of the lemniscal pathway involving the dorsomedial part of the ventroposteromedial thalamic nucleus. By contrast, deeper layers tended to respond faster than superficial layers following ipsilateral stimulations. Such a trend was stronger in plBC, whose L5/6 neurons responded earlier than in amBC (Fig. 2G). This may result from the higher abundance of callosal innervation reaching the plBC that can increase the likelihood of monosynaptic responses in the recorded neuronal pool, thereby shortening the average response onset. The same tendency to show a faster response onset in plBC than in amBC is present for L2/3 (P = 0.0545, d = 0.92, MD = 13.7 ms), which also receives monosynaptic input from contralateral L2/3 in the representation of row A (*39*). Regarding L4, barrel hollows are virtually devoid of functional CC contacts, at least from axons originating in L2/3 of the opposite hemisphere (*39*), while agranular septal compartments are often reported to be the recipient of CC axons in this layer (*17*, *22*, *23*, *51*, *52*), albeit a functional synapse has never been described. Hence, a population trend toward indirect, multisynaptic responses can explain why plBC and amBC responses in L4 have more similar onset delays (Fig. 2G). A stronger input to L5 than to L2/3 of the row A representation characterizes callosal axons originating in L2/3 of the opposite hemisphere (*44*), and L2/3 neurons down-state V_m tends to be more hyperpolarized than the L5/6 one, despite sharing a similar action potential threshold (table S7). Moreover, a previous in vivo study described that L5 neurons show higher input resistance than neuron in upper layers (*53*). These factors may explain the concentration of side-invariant responding neurons in the L5/6 pool (Fig. 6, E and F) and their increased tendency to fire upon ipsilateral stimulation (15 of 24, ~62%) than L2/3. In this vein, the increased amplitude of thalamocortical responses in plBC of callosally projecting L2/3 (Fig. 2, D and E, and fig. S4C) may also contribute to the vigor exhibited by L5/6 ipsilateral responses. Instead, the weaker ipsilateral response of amBC neurons (Fig. 2, F and G) may result from fewer direct callosal connections or from a reduced myelination/caliber of the callosal axons entering this region (see below). In the former case, widespread subthreshold responses may result from inputs travelling via local axon collaterals of neurons monosynaptically connected to the CC, as previously proposed (*3*).

Interhemispheric transmission

In the awake rat, synchronous bilateral stimulation of the whiskers can generate either facilitation or suppression in postsynaptic L5 neuron suprathreshold responses with respect to contralateral stimulation alone (*15*), suggesting a complex form of bilateral integration. On the other hand, ipsilateral stimulation alone generates responses which produce fewer spikes than contralateral ones in S1 (*14*–*16*). Consistent with this fact, in previous (*11*, *12*) and in the present work, most subthreshold ipsilateral responses rose slowly and with a smaller amplitude than their contralateral counterparts, leading to a minor drive for firing. Callosal conduction velocities show great variability (*54*) due to the rich diversity in axonal caliber and myelination (*2*, *3*). Moreover, in the mouse S1, infragranular layers are more extensively myelinated than supragranular ones (*55*), with both compartments containing callosally projecting neurons (*17*). Such heterogeneity may provoke an asynchronous synaptic summation of inputs in postsynaptic neurons translating into a minor drive for spiking. The stimulation of more than one callosal axon belonging to L2/3 neurons led to an asynchronous input summation in postsynaptic row A neurons (*39*). This asynchronous transmission through the CC, more evident in scantily connected areas, transforms the original thalamocortical response of the opposite hemisphere into a sparse barrage of synaptic inputs. This lack of synchrony could be stronger during whisking, as suggested by a previous description of activity desynchronization between BCs that were recorded at BC coordinates roughly corresponding to our amBC ones (*56*). By contrast, increasing the strength of callosal connectivity may mitigate this phenomenon such that thalamocortical activations can be replicated in the opposite hemisphere. In the representation of midline body parts, this neural operation is thought to maintain the continuity between right and left sensory maps (*6*, *9*, *10*). Here, we propose such a scenario for row A-whiskers, which show a significant degree of side-invariant representation in the BC (Fig. 6, A, C, and D), regarding excitatory and inhibitory components of the subthreshold whisker responses (Fig. 6C), evoked spiking activity (Fig. 6, F to H), and the highest degree of callosal innervation spared from developmental pruning (*24*).

Beyond the midline rule in the whisker system

The side-invariant representation of row A-whiskers suggests that they have less discriminative capabilities than remainder whiskers. This is because spatial coding, which relies on the topography of single whiskers within the array (*57*), may be less efficient in discriminating which one of the two rows A contacts an object. This accompanies a difference in muscles′ anchoring to row A-follicles, which lead them to counterrotate during torsion in the whisker cycle with respect to remainder whiskers (*58*, *59*), suggesting a unique role for these rows. Here, we propose two possible scenarios. On the one hand, the side-invariant representation of row A-whiskers may allow the animal to gather positional cues of tactile features belonging to an object in the scanned space with reference to the

facial midline. This is mainly suggested by the organization of the neural pathways. Such maps of the space are most prominently represented by L2/3 and L5 neurons in the BC (*47*), with both compartments projecting/receiving axons trancallosally (*17*). Moreover, plBC at the S1/S2 border receives a more direct heterotopic input than amBC (Fig. 7, G to J) in addition to the homotopic input, thus potentially constituting the earliest connectional hub for the two sensory hemispaces. Last, the S1/S2 border sends ipsi- and contralateral projections to the perirhinal cortex (*25*), a polymodal area involved in object recognition (*60*), where an egocentric map of objects′ features may be built up in association with other modalities. In this manner, the animal could explore objects through the position of their features with respect to its face. A second use of this side-invariant representation of row A-whiskers may be for the easy transformation of the frame of coordinates between body parts lying on the facial midline. These transformations are needed when one system has to approach the same object in the space that another system has detected (*57*). For example, the rows A may allow the animal to accurately position its nose over a tactually salient spot in space. This second interpretation is supported by the exemplary case of the star-nosed mole, whose life heavily relies on palpation. To align the mouth with food, the star-nosed mole performs a "tactile foveation," which is mediated by extremely touch-sensitive, midline appendages interposed between the two nostrils (*61*). Notably, by resembling the row A-whiskers representation in mice and rats, the midline appendages′ S1 representation has the densest callosal innervation among the peers composing the tactile "star" (*62*). Hence, the similarity in sensory modality, midline positioning, and callosal representation may result in an analogous behavioral role in these species.

MATERIALS AND METHODS

Ethical approval

All the experimental procedures were in conformity with the directive 2010/63/EU of the European Parliament and of the Council and the RD 53/2013 Spanish regulation on the protection of animals use for scientific purposes, approved by the government of the Autonomous Community of Valencia, under the supervision of the Consejo Superior de Investigaciones Científicas and the Miguel Hernandez University Committee for Animal use in Laboratory.

Experimental animals

For c-Fos experiments, we used wild-type C57BL6 mice (n = 16) of either sex between 2 and 3 months of age. For electrophysiological experiments, we used wild-type C57BL6 mice (n = 23) and the transgenic line *NEX-Cre* (*44*) (n = 23) mice (donated by K.A. Nave and V. Borrell) of either sex and aged 2 to 6 months. In addition, 14 wild-type C57BL6 mice were used for the extracellular multiunit recordings with silicon probe electrodes. All animals were housed preferentially with cage mates at T = 24°C in our institution′s animal facility with 12-hour daily illumination and food and water ad libitum.

c-Fos immunoassay

To habituate mice to the environment, the first day, they were placed in a covered empty arena (black vinyl material; 50 cm by 50 cm by 70 cm) in complete darkness for ~1 hour. The following day, they were briefly (~15 min) anesthetized with 2 to 4% isoflurane in oxygen (0.8 liters/min) to allow interventions on whisker pads. In trimmed whisker condition, whiskers were trimmed bilaterally, paying attention to reach the very base of the whiskers. For bi- and unilateral lidocaine conditions, lidocaine (150 to 200 μl) was injected subcutaneously, with the volume subdivided in one to two injections to cover the entire whisker pad. We waited 90 to 120 min for the anesthesia to fade completely before testing the mice in the arena in the presence of new objects of various sizes and shapes. Success of lidocaine injections was assessed by visually checking the inability to whisk in the injected side(s) before test. In the majority of experiments, animals were tracked with a Pixy camera to monitor the locomotor performance (fig. S1C). After 45 min of free exploration, mice were euthanized by lethal injection of sodium pentobarbital, transcardially perfused with 4% paraformaldehyde (PFA) in 0.1 M phosphate buffer (pH 7.4), and decapitated, and their brain was extracted. After tangential sectioning and c-Fos immunostaining of flattened cortical preparations, images were acquired with a confocal microscope (Leica SPEII) with 10-μm step-size using a 20× immersion objective. Data from images were quantified using the Fiji software. Area and disposition of regions of interest (ROIs) from barrels and septa were recognized by VGlut2 immunostaining, extracted, and then projected onto the respective image showing the c-Fos channel. In this manner, we could assign the count of immunopositive nuclei to their BC compartments. By dividing the nuclei count for the ROIs area, we obtained a measure of c-Fos$^+$ nuclei density (number of nuclei/0.1 mm^2) in target barrels (A_1-A_4, B_1-B_3, C_1-C_7, D_1-D_7, and E_1-E_7) and septa (A/B, B/C, C/D, and D/E). Anterior BC contained A_4, B_3, C_4-C_7, D_4-D_7, and E_4-E_7 barrels, while posterior BC contained A_1-A_3, B_1-B_2, C_1-C_3, D_1-D_3, and E_1-E_3 barrels. In lidocaine cohorts, if the contralateral BC showed c-Fos expression clearly resembling the one of thalamocortical activation (i.e., very dense c-Fos labeling within the barrel hollow) in the barrels of interest, then the lidocaine effect was considered faded before sacrifice, and mice were excluded from the analysis. Count in missing barrels of histological sections was replaced by NaN (Not a Number).

Viral injections

To impose the activation of callosal projection neurons, we infected pyramidal cells of the right BC with AAV viral vectors encoding optogenetic tools. Anesthesia (2 to 4% isoflurane in oxygen, 0.8 liters/min) was induced and maintained for the course of the surgery in *NEX-Cre* mice immobilized in a stereotaxic apparatus (Kopf Instrument). Lidocaine cream was applied to the skin over the skull before opening, and eyes were covered with ophthalmic gel (Viscotears, 2 mg/g) to prevent corneal desiccation. Analgesic (Metacam, 0.4 ml) was delivered by intraperitoneal injection. Craniotomy was drilled either at coordinates anteroposterior (AP) −2, mediolateral (ML) −3.8 (plBC) or AP −1 ML −3.2 (amBC) from bregma, exposing the dura mater. The ssAAV-5/2-hEF1α-dlox-hChR2(H134R)_EYFP(rev)-dlox-WPRE-hGHp(A) viral construct (ETH Zurich) was injected in small volumes (100 to 200 nl) at 0.7-mm depth with a precision injector (Nanoliter, World Precision Instruments). Skin was then closed with surgical glue, and animals rested in a recovery chamber until restoration of normal locomotor activity.

Immunohistochemistry

After every experiment, mice were perfused with 4% PFA. Their brains were postfixed also in 4% PFA for 2 hours at room temperature and then stored at 4°C in phosphate-buffered saline (PBS) with 30% sucrose plus 0.1% sodium azide before their use. For flattened preparations of the cortex, the entire cortical mantle was isolated from the brain and pressed overnight in a custom-made, plastic press-and-hold apparatus of 1-mm depth in a 4% PFA bath before sectioning. Tangential slices 80-μm thick from flattened cortex and coronal slices 50-μm thick from intact brains were cut with a digital cryotome (Microm HM450; Thermo Fisher Scientific). After washing with PBS, sections were exposed to a blocking solution of 0.1 M PBS with 1% bovine serum albumin (BSA) and 0.5% Triton X-100 for 2 hours at room temperature. Next, they were incubated overnight with primary antibodies (4°C) diluted in blocking solution. To stain thalamocortical afferents for recognizing L4 barrels, we used guinea pig anti-VGlut2 (1:4000; Synaptic Systems). To detect c-Fos expressing nuclei, we used rabbit anti-cFos (1:700; Synaptic Systems). The following day, sections were washed and incubated for 2 hours at room temperature in blocking solution with secondary antibodies, adding streptavidin for tissues previously used in electrophysiological experiments (see below). Once this time elapsed, they were mounted on microscope slides (Menzel-Gläser Superfrost Plus; Thermo Fisher Scientific), covered with mowiol (Calbiochem) and coverslipped (Menzel-Gläser; Thermo Fisher Scientific). To recover biocytin-filled neurons from electrophysiological experiments, we used Cy2- or Cy3-conjugated streptavidin (Jackson ImmunoResearch Laboratories), diluted, respectively, 1:500 and 1:1000 in blocking solution. As secondary antibodies, we used goat anti-guinea pig Alexa Fluor 568 and 633 (Thermo Fisher Scientific), both with 1:500 dilutions, and donkey anti-rabbit Alexa Fluor 488 (Thermo Fisher Scientific) at dilution 1:500, and 4′,6-diamidino-2-phenylindole (Thermo Fisher Scientific) for nuclei. For cell recovery in amBC recordings, coronal sections were collected from bregma AP −0.58 to AP −1.58, while for plBC from bregma AP −1.82 to AP −2.30 [following (*63*)].

In a set of experiments, SOM^+ and PV^+ GABAergic interneurons were labeled by immuhistochemistry. In addition to the procedures described above, brains were covered in 4% agarose and cut with a vibratome (VT1000 S; Leica). Then, slices were submerged in a solution containing 1% BSA, 0.1% Triton X-100, and 4% donkey serum diluted in PBS for 2 hours at room temperature. After that, samples were incubated overnight in PBS with 1% BSA, 0.1% Triton X-100, 1% donkey serum, and primary antibodies. These were rat anti-somatostatin (1:400; Merck), rabbit anti-parvalbumin (1:2000; Swant Inc.), and guinea pig anti-VGlut2 (1:4000; Synaptic Systems). Next day, the samples were washed (3 × 10 min) and incubated for 2 hours at room temperature in a PBS solution with the secondary antibodies, in this case: anti-rat Alexa Fluor 647 (Jackson ImmunoResearch) for somatostatin, anti-guinea pig Alexa Fluor 633 (Invitrogen) for parvalbumin, and anti-guinea pig Alexa Fluor 568 (Invitrogen) for Vglut2.

Axonal tracing and interneuron quantification

To label callosal projections in left BC subregions, we injected 200 nl of 10% BDA in the right hemisphere either in the plBC (AP −2, ML 3.9) or the amBC (AP −1, ML 2.8) subregion. After 1 week, animals were perfused with 4% PFA, and brains were stored at 4°C in 4% PFA overnight. As above, 50-μm-thick coronal cryosections were incubated overnight with pig anti-VGlut2 (1:4000; Synaptic Systems), followed the second day by the application of goat anti-guinea pig Alexa Fluor 633 (1:500; Thermo Fisher Scientific) and Cy2-conjugated streptavidin (1:500; Jackson ImmunoResearch). Pictures were taken with the Thunder microscope (dry, 10×; Leica Microsystems). For each brain, seven pictures were taken: one image of the section with the highest fluorescence at the injection site, three consecutive sections containing the row E barrels (amBC), and three consecutive sections containing the row A barrels (plBC). Two different ROIs were drawn with ImageJ: one comprising the whole column of the rows A/B whiskers (AP −2; ML 3.5 to 4) and another comprising the whole column of the rows D/E (AP −1; ML 2.75 to 3.25). Images were then binarized with Otsun′s threshold, and in each ROI, the number of pixels corresponding to BDA fluorescence was quantified. We estimated the callosal fibers′ density by the number of fluorescent pixels divided by the total number of pixels of the ROI. Normalization of the data was performed by dividing each density value by the average density of the injection ROI.

Images of PV^+ and SOM^+ interneurons were obtained using a fluorescence microscope (Thunder Leica Microsystems). Four images of consecutive sections corresponding to the amBC and plBC zones were taken for each hemisphere. For each slice, a Z-stack was created using images every 8 μm, and the maximum projection intensity was used to obtain a single image. amBC and plBC regions were selected according to the coordinates described in *28* and following Paxinos Mouse Brain Atlas (AP −2; ML 3.5 to 4 and AP −1; ML 2.75 to 3.25 respectively). For each hemisphere, two different ROIs were drawn for ImageJ software: one delimiting the whole column of A/B whiskers and another encompassing the whole columns of the rows D/E. Then, the images were preprocessed using a median filter. Afterward, the images were binarized using a threshold (mean + 3 SD). Quantification of the number of cells was performed through a costume code in Phyton, using opencv-python library. The data were normalized dividing the number of cells by the ROIs area.

Whiskers and optogenetic stimulation

With the exception of the pairs A_2-A_3 and E_2-E_3, whiskers were trimmed bilaterally at their base to avoid any unintended stimulation accompanying the one of target whiskers. Spared whiskers, separately for each row (i.e., A and E), were glued together with super glue along their length. Then, they were attached to the tip of Teflon-coated stainless wire of a custom-made solenoid puller (see fig. S8A) with super glue. In this manner, and depending on the target cortical area (i.e., plBC or amBC), mirror whiskers of both sides of the snout were connected to the solenoid puller. Whiskers′ stimulation consisted of fast caudo-rostral axis displacement (~3.5 mm) lasting 15 ms, delivered every 3 or 5 s, contra- and ipsilateral to the patch-clamp recording electrode. For optogenetic experiments in *NEX-Cre* mice, single step-like photostimulations lasting 5 or 10 ms were delivered every 3 or 5 s, with an optic fiber (400 μm in diameter) connected to a blue light source (Prizmatix LED, 453-nm wavelength, 3.76-mW light power) and governed by the CED 1401 (Power 3) through a custom-made program (Spike2). Two craniotomies were drilled. The fiber tip was positioned perpendicular to the surface of the brain within the craniotomy used for delivering the viral construct, either at plBC or amBC coordinates. A micro-holding device (*64*) was used

to keep in the same coordinate the borosilicate capillary (1B150F-4, WPI) containing the LFP electrode and the optic fiber, except that the tip of the electrode was deepened 1 mm into the cortex, while the optic fiber rested on the brain surface. In the second, fiber-free craniotomy, another LFP electrode (0.9 to 1.2 megohm), was placed at 1-mm depth into the cortex to check for the anatomical specificity of the optogenetic activation. Mirror- and nonmirror LFPs were considered jointly active in BC_{wide} stimulations if their negative deflection in response to optogenetic illumination surpassed 400 μV (Fig. 7F).

TTX experiments

The disposition of plBC and amBC LFPs was similar to the optogenetic settings, except that the fiber inserted in the micro-holder was replaced by a borosilicate capillary with broken tip, containing 1 to 1.5 μl of TTX 100 μM. TTX was released through positive pressure at 1-mm cortical depth in plBC. Responses to ipsilateral row A-whisker stimulation were analyzed after that, from plBC, the depression of activity reached the electrode in amBC (Fig. 4A).

Electrophysiological recordings

Electrophysiological recordings were performed on top of an air table for vibration cancellation (CleanBench, TMC). Mice were head-fixed in a customized stereotaxic apparatus with ear bars (Stoelting). We induced anesthesia by intraperitoneal injection of ketamine (75 mg/kg) and medetomidine (1 mg/kg) diluted in 0.9% NaCl saline solution. One third of the original dose was injected intramuscularly to maintain anesthesia once paw reflex could be evoked or the LFP trace exhibited signatures of awakening. To avoid mechanical instability induced by respiration, a tracheotomy was performed before animal immobilization in the stereotaxic apparatus. A tube blowing oxygen-enriched air was placed ~1 cm in front of the cannula, previously inserted in the trachea. The animal rested over a heating pad governed by a thermostat (FHC Inc.) to maintain core body temperature at 36.5 ± 0.5°C. Depending on the experiment, two to three circular craniotomies were drilled over the BCs (~5 mm in diameter). Typically, they were one per hemisphere at mirror symmetric coordinates (reported in the "Viral injections" section), plus another in the right hemisphere when required, to host a second LFP at nonmirror symmetric coordinates with respect to the contralateral (left hemisphere) patch-clamp electrode. Craniotomies were constantly kept wet by application of 0.9% NaCl solution for the entire recording duration. In the craniotomy for patch-clamp, we gently removed the dura with a syringe needle bent at the tip and stopped eventual bleeding with cotton sticks. To approach the cortical representation of target whiskers within plBC or amBC craniotomies, we delivered contralateral stimulations of the whiskers group matching its cortical representation, respectively, the pair A_2-A_3 for plBC and E_2-E_3 for amBC. A borosilicate capillary filled with 0.9% NaCl solution contained a LFP electrode (0.9 to 1.2 megohm). We used this to navigate the craniotomy through a digital micromanipulator (Luigs & Neumann, set at 1-μm precision) for sampling cortical responses to whiskers' stimulations on the dura's surface. After that, the average of 10 to 20 LFP responses was calculated online by the software (Spike2), the electrode was moved to the next position within the craniotomy, and the process was repeated (fig. S8C). After three to six loci sampled, by visually comparing the averages obtained, the one with the strongest initial negative deflection was chosen to be the location for patch-clamp recordings. In particular in younger animals (PD ~60), these loci could be also recognized on the brain surface with reference to brain vessels. For patch-clamp recordings, we used an angle of ~60°. Cortical depth of the recording was collected through display reading of the micromanipulator (1-μm step size). By comparing our histological preparations with display readings and the bibliography [especially *39*)], we considered as L2/3 neurons recorded between 101 and 300 μm from the pia, as L4 the ones recorded between 301 and 500 μm, and L5/6 neurons below 501 μm until the white matter, at approximately 1100 μm. After anatomical recovery of biocytin-filled neurons, these coordinates associated with the penetration angle showed to be optimal for neurons recorded in plBC. However, for recordings in amBC, a more perpendicular angle would have been required. In fig. S8D, we provide the details of the correction procedure for depth in amBC. Pipettes for patch-clamp recordings (7 to 11 megohm) were back-filled with intracellular solution containing 125 mM K-gluconate, 10 mM KCl, 10 mM Na-phosphocreatine, 10 mM Hepes, 4 mM adenosine triphosphate–Mg, and 0.3 mM guanosine triphosphate–Na. pH and osmolality were adjusted to ~7.4 and ~280 mOsm/liter, respectively. Biocytin (0.2 to 0.4%, Sigma-Aldrich) was then added to the intracellular solution to recover the recorded cell after every experiment (Fig. 2B). Borosilicate capillaries, both used for LFP or patch-clamp recordings, were pulled with a micropipette puller (Flaming/Brown P-1000, Sutter Instrument). Recorded signals were amplified with MultiClamp 700B (Molecular Devices), converted to digital with a CED 1401 (Power 3) acquisition board at 20 KHz, and streamed to a laptop (Windows 10) running Spike2 software (Cambridge Electronics Design). At the end of each experiment, mice were euthanized with a lethal intraperitoneal injection of pentobarbital, perfused transcardially with 4% PFA in 0.1 M phosphate buffer (pH 7.4), and decapitated, and their brains were extracted and postfixed overnight in 4% PFA. Thus, brains were maintained in 30% sucrose solution with sodium azide at 4°C until the sectioning day. In this study, we recorded intracellularly a total of 110 left-BC neurons from 54 mice (~2 neurons per mouse), including histologically recovered and unrecovered neurons. Of this pool, whisker responses were obtained from 75 neurons, and optogenetic responses from 45 neurons, 10 of which also underwent sensory stimulation. Two L4 neurons have been excluded for very long response delays [>15 ms; see (*45*)], indicating that the recording was misplaced. Moreover, we could clearly detect only two putative fast-spiking neurons in our pool (~3%) by the remarkably short spike half-width (<0.7 ms; population median: 1.15 ms). Yet, their proportion has to be higher since the normally reported proportion is 10 to 15% for the rodent neocortex (*65*). The two putative fast-spiking neurons were included in the analysis.

In a subset of experiments (Fig. 4, F to H, $n = 6$; fig. S4, $n = 8$), extracellular activity was recorded in plBC and amBC along the cortical columns, using 2 linear silicon probe electrodes (NeuroNexus Technologies, Ann Arbor, MI). Shanks were inserted perpendicular to the cortex, each one contained eight electrodes, spaced by 200 μm. Data were continuously digitized at 20 kHz using a SmartBox V2 amplifier (NeuroNexus Technologies, Ann Arbor, MI).

Data analysis

We analyzed data with MATLAB 2015a (MathWorks). First, we down-sampled acquired signals to 10 KHz. Then, we isolated

spontaneous up- and down-states of the V_m through a moving average window, considering up-state V_m values exceeding a threshold obtained by summing the mean V_m within the moving window to 0.4 times V_m SD and down-states the values below this threshold. BC up-states often display complex shapes, characterized by two or more peaks (*66*). Thus, short hyperpolarizing events (<150 ms) falling below the threshold and thus classified as brief down-states were elided and considered voltage excursions within up-states. Analogously, too-short depolarizing events (<15 ms) misclassified as up-state were included in down-state. Neural responses to whiskers and optogenetic stimulations were isolated from 200 ms before to 500 ms after the stimulation trigger. We selected responses in down-state only for stimulations falling 100 ms after the end of an up-state. Both kinds of responses were spike-filtered with a median plus the Savitzky-Golay filters (MATLAB functions: *medfilt1* and *sgolayfilt*) applied in this order. For every neuron, we obtained the waveform average through the mean of the spike-filtered responses, with spikes vectors collected separately. Onset delay of responses in down-state was defined as the delay between stimulation delivery (digital trigger) and threshold crossing by the V_m. Threshold was defined as the mean V_m during 50 ms of down-state preceding stimulation multiplied by 50 times its SD. Peak delay was defined as the difference between stimulation delivery and the V_m maximal amplitude time points, within 300-ms post-stimulation. Amplitude was defined as the V_m difference between the peak of the spike-filtered response and the prestimulus baseline (i.e., down-state or resting V_m). Half amplitude delay was defined as the time between stimulation delivery and response peak. Slope of the rising phase was defined as the angular coefficient of the first-degree polynomial fitted to the waveform average in the time between onset and peak delay (MATLAB function: *fit*). These measures were visually assessed on the waveform averages and manually adjusted when needed. Probability of action potential firing [P(AP)] was calculated in a poststimulus time window of 50 ms for contra- and 80 ms for ipsilateral responses, by dividing the number of times that a neuron fired at least one spike following stimulation by the total number of stimulations delivered. A given neuron was classified as spike responding if it had a P(AP) > 0. In intracellular recordings, firing rate was computed with 20-ms bins in response to each stimulation of a protocol and the maximum extracted, yielding the maximal firing rate (max FR). Amplitude of downward deflections of the LFPs (spontaneous up-states) was obtained by smoothing the signal and using *findpeaks* in MATLAB, thus averaging the values for single recordings, separately for CTRL and TTX. Peak delay, amplitude and slope were *z*-scored to measure the Mahalanobis distance between homotopic ipsi- and contralateral responses in plBC or amBC, both for excitatory and inhibitory components (MATLAB function: *mahal*). Distance values are provided as the square root of the function output (given in squared values). Cross-correlation coefficients between ipsi- and contralateral responses were calculated in the 400 ms after stimulation (MATLAB function: *xcorr*), limiting the lag range to ±50 ms. Membrane properties were calculated from negative and positive injection currents (i.e., from −100 to 100 nA, by 14 increasingly positive steps) delivered to neurons during spontaneous activity, separately for up- and down-states. Membrane constant τ (milliseconds) was defined as the time at which the membrane potential reached the 37% of its resting value upon current injection, averaged through negative and positive current steps. We obtained the resistance (megohm) through the angular coefficient of the first-degree polynomial fitted to V_m values receiving the current injections and separately calculated the values for up- (R_{up}) and down-states (R_{down}). We measured the cells' capacitance (picofarad) by dividing τ for the resistance in up- (C_{up}) and down-states (C_{down}).

Last, recordings obtained by the silicon probes (fig. S4) were imported and analyzed offline using Python. The raw data signals were down-sampled to 10 kHz and filtered (Butterworth bandpass filter, 0.6 to 3 kHz, order 5), and multiunit activity was extracted by applying a threshold at five times the SD of 10 min for each recording. Relative to the stimulus trigger, the peristimulus time histograms were calculated with a resolution of 5-ms bins. The amplitude of the peak response was estimated as the maximum number of spikes per bin occurring after stimulus onset. The peak response ratio was calculated by dividing the peak amplitude of ipsilateral responses by the peak amplitude of the contralateral ones. Peak delay was defined as the time it took for the response to reach its maximal amplitude.

Statistics

Graphs, quantification, and statistical tests have been performed in MATLAB R2015a (MathWorks). Values are expressed as median (25th to 75th quantiles), with the median graphically represented by a red dot and the mean by a black square ± SEM (whiskers). Violin plots showing the median (red line) and quartiles (dashed lines) have been obtained with GraphPad Prism 8. We used a two-sided Wilcoxon rank sum test for statistical comparison of unmatched samples and two-sided Wilcoxon signed-rank (WSR) test for matched samples. To test the homogeneity of distributions, we used the χ^2 test and the tabulated values to infer statistical significance, applying the Yate's correction for df = 1. Effect size was expressed as the mean difference in SD units, indicated as *d*. MD indicates difference between medians. For comparisons involving more than two sample distributions, we used Kruskal-Wallis (KW) test with Fisher's least square difference (LSD) post hoc test to infer statistical significance of pairwise comparisons. We applied the Bonferroni-Holm correction in multiple comparisons. For all statistical tests, the null hypothesis was rejected at the 5% significance level. $^*P < 0.05$, $^{**}P < 0.01$, and $^{***}P < 0.001$.

Supplementary Materials

This PDF file includes:

Tables S1 to S7
Figs. S1 to S8

REFERENCES AND NOTES

1. R. Suárez, I. Gobius, L. J. Richards, Evolution and development of interhemispheric connections in the vertebrate forebrain. *Front. Hum. Neurosci.* **8**, 497 (2014).
2. G. M. Innocenti, General organization of callosal connections in, *the cerebral cortex. In Sensory-motor areas and aspects of cortical connectivity*, (Springer, 1986), pp. 291–353.
3. F. Conti, T. Manzoni, The neurotransmitters and postsynaptic actions of callosally projecting neurons. *Behav. Brain Res.* **64**, 37–53 (1994).
4. R. E. Myers, R. W. Sperry, Interhemispheric communication through the corpus Callosum. *AMA Arch. Neurol. Psychiatry* **80**, 298–303 (1958).
5. G. Berlucchi, G. Rizzolatti, Binocularly driven neurons in visual cortex of split-chiasm cats. *Science* **159**, 308–310 (1968).
6. T. Manzoni, P. Barbaresi, F. Conti, M. Fabri, The callosal connections of the primary somatosensory cortex and the neural bases of midline fusion. *Exp. Brain Res.* **76**, 251–266 (1989).

7. Y. Iwamura, Bilateral receptive field neurons and callosal connections in the somatosensory cortex. *Philos. Trans. R. Soc. Lond. B Biol. Sci.* **355**, 267–273 (2000).
8. F. Aboitiz, J. Montiel, One hundred million years of interhemispheric communication: The history of the corpus callosum. *Braz. J. Med. Biol. Res.* **36**, 409–420 (2003).
9. J. C. Houzel, M. L. Carvalho, R. Lent, Interhemispheric connections between primary visual areas: Beyond the midline rule. *Braz. J. Med. Biol. Res.* **35**, 1441–1453 (2002).
10. Ramón y Cajal, S. (1898). Estructura del quiasmo óptico y teoria general de los entrecruzamientos nerviosos. Revista Trimestral Micrográfica, 3: 2–18.
11. I. D. Manns, B. Sakmann, M. Brecht, Sub- and suprathreshold receptive field properties of pyramidal neurones in layers 5A and 5B of rat somatosensory barrel cortex. *J. Physiol.* **556**, 601–622 (2004).
12. R. Reig, G. Silberberg, Multisensory integration in the mouse striatum. *Neuron* **83**, 1200–1212 (2014).
13. R. Reig, G. Silberberg, Distinct corticostriatal and intracortical pathways mediate bilateral sensory responses in the striatum. *Cereb. Cortex* **26**, 4405–4415 (2016).
14. M. G. Shuler, D. J. Krupa, M. A. Nicolelis, Bilateral integration of whisker information in the primary somatosensory cortex of rats. *J. Neurosci.* **21**, 5251–5261 (2001).
15. M. C. Wiest, N. Bentley, M. A. L. Nicolelis, Heterogeneous integration of bilateral whisker signals by neurons in primary somatosensory cortex of awake rats. *J. Neurophysiol.* **93**, 2966–2973 (2005).
16. A. Pala, G. B. Stanley, Ipsilateral stimulus encoding in primary and secondary somatosensory cortex of awake mice. *J. Neurosci.* **42**, 2701–2715 (2022).
17. S. P. Wise, E. G. Jones, The organization and postnatal development of the commissural projection of the rat somatic sensory cortex. *J. Comp. Neurol.* **168**, 313–343 (1976).
18. K. A. Koralek, H. P. Killackey, Callosal projections in rat somatosensory cortex are altered by early removal of afferent input. *Proc. Natl. Acad. Sci.* **87**, 1396–1400 (1990).
19. K. Sehara, T. Toda, L. Iwai, M. Wakimoto, K. Tanno, Y. Matsubayashi, H. Kawasaki, Whisker-related axonal patterns and plasticity of layer 2/3 neurons in the mouse barrel cortex. *J. Neurosci.* **30**, 3082–3092 (2010).
20. C.-L. Wang, L. Zhang, Y. Zhou, J. Zhou, X.-J. Yang, S.-M. Duan, Z.-Q. Xiong, Y.-Q. Ding, Activity-dependent development of callosal projections in the somatosensory cortex. *J. Neurosci.* **27**, 11334–11342 (2007).
21. R. Suárez, L. R. Fenlon, R. Marek, L. Avitan, P. Sah, G. J. Goodhill, L. J. Richards, Balanced interhemispheric cortical activity is required for correct targeting of the corpus callosum. *Neuron* **82**, 1289–1298 (2014).
22. J. Olavarria, R. C. Van Sluyters, H. P. Killackey, Evidence for the complementary organization of callosal and thalamic connections within rat somatosensory cortex. *Brain Res.* **291**, 364–368 (1984).
23. K. A. Koralek, J. Olavarria, H. P. Kellackey, Areal and laminar organization of corticocortical projections in the rat somatosensory cortex. *J. Comp. Neurol.* **299**, 133–150 (1990).
24. J. Zhou, Y. Lin, T. Huynh, H. Noguchi, J. O. Bush, S. J. Pleasure, NMDA receptors control development of somatosensory callosal axonal projections. *eLife* **10**, e59612 (2021).
25. L. R. Fenlon, R. Suárez, L. J. Richards, The anatomy, organisation and development of contralateral callosal projections of the mouse somatosensory cortex. *Brain Neurosci Adv* **1**, 239821281769488 (2017).
26. R. K. Filipkowski, M. Rydz, B. Berdel, J. Morys, L. Kaczmarek, Tactile experience induces c-fos expression in rat barrel cortex. *Learn. Mem.* **7**, 116–122 (2000).
27. T. Gener, R. Reig, M. V. Sanchez-Vives, A new paradigm for the reversible blockage of whisker sensory transmission. *J. Neurosci. Methods* **176**, 63–67 (2009).
28. P. M. Knutsen, C. Mateo, D. Kleinfeld, Precision mapping of the vibrissa representation within murine primary somatosensory cortex. *Philos. Trans. R. Soc. Lond. B Biol. Sci.* **371**, 20150351 (2016).
29. D. J. Krupa, A. J. Brisben, M. A. Nicolelis, A multi-channel whisker stimulator for producing spatiotemporally complex tactile stimuli. *J. Neurosci. Methods* **104**, 199–208 (2001).
30. C. C. Petersen, T. T. Hahn, M. Mehta, A. Grinvald, B. Sakmann, Interaction of sensory responses with spontaneous depolarization in layer 2/3 barrel cortex. *Proc. Natl. Acad. Sci.* **100**, 13638–13643 (2003).
31. R. Reig, M. V. Sanchez-Vives, Synaptic transmission and plasticity in an active cortical network. *PLOS ONE* **2**, e670 (2007).
32. J. F. Staiger, K. Zilles, T. F. Freund, Distribution of GABAergic elements postsynaptic to ventroposteromedial thalamic projections in layer IV of rat barrel cortex. *Eur. J. Neurosci.* **8**, 2273–2285 (1996).
33. Z. Tan, H. Hu, Z. J. Huang, A. Agmon, Robust but delayed thalamocortical activation of dendritic-targeting inhibitory interneurons. *Proc. Natl. Acad. Sci.* **105**, 2187–2192 (2008).
34. L. Gabernet, S. P. Jadhav, D. E. Feldman, M. Carandini, M. Scanziani, Somatosensory integration controlled by dynamic thalamocortical feed-forward inhibition. *Neuron* **48**, 315–327 (2005).
35. W. B. Wilent, D. Contreras, Dynamics of excitation and inhibition underlying stimulus selectivity in rat somatosensory cortex. *Nat. Neurosci.* **8**, 1364–1370 (2005).
36. Y. Kawaguchi, Receptor subtypes involved in callosally-induced postsynaptic potentials in rat frontal agranular cortex in vitro. *Exp. Brain Res.* **88**, 33–40 (1992).
37. P. G. Anastasiades, J. J. Marlin, A. G. Carter, Cell-type specificity of callosally evoked excitation and feedforward inhibition in the prefrontal cortex. *Cell Rep.* **22**, 679–692 (2018).
38. C. Rock, A. J. Apicella, Callosal projections drive neuronal-specific responses in the mouse auditory cortex. *J. Neurosci.* **35**, 6703–6713 (2015).
39. L. Petreanu, D. Huber, A. Sobczyk, K. Svoboda, Channelrhodopsin-2–assisted circuit mapping of long-range callosal projections. *Nat. Neurosci.* **10**, 663–668 (2007).
40. D. A. Steindler, Trigeminocerebellar, trigeminotectal, and trigeminothalamic projections: A double retrograde axonal tracing study in the mouse. *J. Comp. Neurol.* **237**, 155–175 (1985).
41. T. Fukushima, F. W. Kerr, Organization of trigeminothalamic tracts and other thalamic afferent systems of the brainstem in the rat: Presence of gelatinosa neurons with thalamic connections. *J. Comp. Neurol.* **183**, 169–184 (1979).
42. R. S. Erzurumlu, Y. Murakami, F. M. Rijli, Mapping the face in the somatosensory brainstem. *Nat. Rev. Neurosci.* **11**, 252–263 (2010).
43. T. Hayama, H. Ogawa, Regional differences of callosal connections in the granular zones of the primary somatosensory cortex in rats. *Brain Res. Bull.* **43**, 341–347 (1997).
44. S. Goebbels, I. Bormuth, U. Bode, O. Hermanson, M. H. Schwab, K. A. Nave, Genetic targeting of principal neurons in neocortex and hippocampus of NEX-Cre mice. *Genesis* **44**, 611–621 (2006).
45. M. Brecht, B. Sakmann, Dynamic representation of whisker deflection by synaptic potentials in spiny stellate and pyramidal cells in the barrels and septa of layer 4 rat somatosensory cortex. *J. Physiol.* **543**, 49–70 (2002).
46. M. Brecht, A. Roth, B. Sakmann, Dynamic receptive fields of reconstructed pyramidal cells in layers 3 and 2 of rat somatosensory barrel cortex. *J. Physiol.* **553**, 243–265 (2003).
47. S. R. Pluta, E. H. Lyall, G. I. Telian, E. Ryapolova-Webb, H. Adesnik, Surround integration organizes a spatial map during active sensation. *Neuron* **94**, 1220–1233.e5 (2017).
48. J. Brown, I. A. Oldenburg, G. I. Telian, S. Griffin, M. Voges, V. Jain, H. Adesnik, Spatial integration during active tactile sensation drives orientation perception. *Neuron* **109**, 1707–1720.e7 (2021).
49. G. Plomp, C. M. Michel, C. Quairiaux, Systematic population spike delays across cortical layers within and between primary sensory areas. *Sci. Rep.* **7**, 15267 (2017).
50. J. C. Nussbaumer, H. Van der Loos, An electrophysiological and anatomical study of projections to the mouse cortical barrelfield and its surroundings. *J. Neurophysiol.* **53**, 686–698 (1985).
51. R. M. Akers, H. P. Killackey, Organization of corticocortical connections in the parietal cortex of the rat. *J. Comp. Neurol.* **181**, 513–537 (1978).
52. L. Záborszky, J. R. Wolff, Distribution patterns and individual variations of callosal connections in the albino rat. *Anat. Embryol.* **165**, 213–232 (1982).
53. W.-J. Zhao, J. Kremkow, J. F. Poulet, Translaminar cortical membrane potential synchrony in behaving mice. *Cell Rep.* **15**, 2387–2399 (2016).
54. Y. Cissé, F. Grenier, I. Timofeev, M. Steriade, Electrophysiological properties and input-output organization of callosal neurons in cat association cortex. *J. Neurophysiol.* **89**, 1402–1413 (2003).
55. G. S. Tomassy, D. R. Berger, H. H. Chen, N. Kasthuri, K. J. Hayworth, A. Vercelli, P. Arlotta, Distinct profiles of myelin distribution along single axons of pyramidal neurons in the neocortex. *Science* **344**, 319–324 (2014).
56. Y. Oran, Y. Katz, M. Sokoletsky, K. C. K. Malina, I. Lampl, Reduction of corpus callosum activity during whisking leads to interhemispheric decorrelation. *Nat Comm* **12**, 4095 (2021).
57. P. M. Knutsen, E. Ahissar, Orthogonal coding of object location. *Trends Neurosci.* **32**, 101–109 (2009).
58. P. M. Knutsen, A. Biess, E. Ahissar, Vibrissal kinematics in 3D: Tight coupling of azimuth, elevation, and torsion across different whisking modes. *Neuron* **59**, 35–42 (2008).
59. S. Haidarliu, K. Bagdasarian, N. Shinde, E. Ahissar, Muscular basis of whisker torsion in mice and rats. *Anat. Rec.* **300**, 1643–1653 (2017).
60. E. A. Murray, B. J. Richmond, Role of perirhinal cortex in object perception, memory, and associations. *Curr. Opin. Neurobiol.* **11**, 188–193 (2001).
61. K. C. Catania, F. E. Remple, Tactile foveation in the star-nosed mole. *Brain Behav. Evol.* **63**, 1–12 (2004).
62. C. K. Catania, J. H. Kaas, Areal and callosal connections in the somatosensory cortex of the star-nosed mole. *Somatosens. Mot. Res.* **18**, 303–311 (2001).
63. G. Paxinos, K. B. J. Franklin, in *The Mouse Brain in Stereotaxic Coordinates* (Academic Press, San Diego, ed. 2, 2001).
64. M. Sáez, M. Ketzef, J. Alegre-Cortés, R. Reig, G. Silberberg, A new Micro-holder device for local drug delivery during in vivo whole-cell recordings. *Neurosci* **381**, 115–123 (2018).
65. R. Tremblay, S. Lee, B. Rudy, GABAergic interneurons in the neocortex: From cellular properties to circuits. *Neuron* **91**, 260–292 (2016).

66. J. Alegre-Cortés, M. Sáez, R. Montanari, R. Reig, Medium spiny neurons activity reveals the discrete segregation of mouse dorsal striatum. *eLife* **10**, e60580 (2021).

Acknowledgments: We are grateful to K.A. Nave and V. Borrell for the transgenic line *NEX-Cre* (*44*), N. Anton-Bolaños for initiating R.M. to the immunohistochemistry of the BC. We thank V. Rodriguez-Milan of the Instituto de Neurociencias workshop for helping with the construction of the whiskers stimulator. We are also grateful to J. Esteve-Agraz for help with the design of some figures. Last, we want to thank E. Geijo, J. Pérez-Fernández, J. de los Reyes Aguilar, I. Pérez-Otaño, and K. Caref for critical reading, discussions, and suggestions on this article. **Funding:** The study was supported by MINECO (PGC2018-094457-B-I00) and CSIC-Severo Ochoa Excellence Programmes of the Instituto de Neurociencias (SEV-2013-0317 and SEV-2017-0723). R.M. was supported by la Caixa-Severo Ochoa programme (2016/00006/001). A.A-A. and I.N. were supported by the ACIF-GVA programme. J.A.-C. was supported by the CSIC-Severo Ochoa Excellence Programme of the Instituto de Neurociencias (SEV2013-0317). **Author contributions:** Conceptualization: R.M. and R.R. Methodology: R.M., J.A.-C., and R.R. Investigation: R.M., J.A.-C., A.A.-A., J.C.-M., I.N., C.G.-F., M.S., and R.R. Visualization: R.M., J.A.-C., A.A.-A., and I.N. Supervision: R.R. Writing—manuscript: R.M. and R.R. Writing—review and editing: R.M., J.A.-C., and R.R. **Competing interests:** The authors declare that they have no competing interests. **Data and materials availability:** All data needed to evaluate the conclusions in the paper are present in the paper and/or the Supplementary Materials. In addition, all data generated during and/or analyzed during the current study are available online at CSIC public repository (DIGITAL.CSIC), following this link: https://doi.org/10.20350/digitalCSIC/15606.

Submitted 21 April 2023
Accepted 27 October 2023
Published 29 November 2023
10.1126/sciadv.adi3728